

MULTI-OBJECTIVE BAYESIAN OPTIMIZATION FOR LIKELIHOOD-FREE INFERENCE IN SEQUENTIAL SAMPLING MODELS OF DECISION MAKING

BY DAVID CHEN^{1,a}, XINWEI LI^{2,c} EUI-JIN KIM^{3,e}
PRATEEK BANSAL^{2,d} AND DAVID NOTT^{1,b}

¹*Department of Statistics and Data Science, National University of Singapore, a1039688@u.nus.edu; bstandj@nus.edu.sg*

²*Department of Civil and Environmental Engineering, National University of Singapore, cxinwei.li@u.nus.edu;
dprateekb@nus.edu.sg*

³*Department of Transportation Systems Engineering, Ajou University, euijin@ajou.ac.kr*

Joint modeling of different data sources in decision-making processes is crucial for understanding decision dynamics in consumer behavior models. Sequential Sampling Models (SSMs), grounded in neuro-cognitive principles, provide a systematic approach to combining information from multi-source data, such as those based on response times and choice outcomes. However, parameter estimation of SSMs is challenging due to the complexity of joint likelihood functions. Likelihood-Free inference (LFI) approaches enable Bayesian inference in complex models with intractable likelihoods, like SSMs, and only require the ability to simulate synthetic data from the model. Extending a popular approach to simulation efficient LFI for single-source data, we propose Multi-objective Bayesian Optimization for Likelihood-Free Inference (MOBOLFI) to estimate the parameters of SSMs calibrated using multi-source data. MOBOLFI models a multi-dimensional discrepancy between observed and simulated data, using a discrepancy for each data source. Multi-objective Bayesian Optimization is then used to ensure simulation efficient approximation of the SSM likelihood. The use of a multivariate discrepancy allows for approximations to individual data source likelihoods in addition to the joint likelihood, enabling both the detection of conflicting information and a deeper understanding of the importance of different data sources in estimating individual SSM parameters. We illustrate the advantages of our approach in comparison with the use of a single discrepancy in a simple synthetic data example and an SSM example with real-world data assessing preferences of ride-hailing drivers in Singapore to rent electric vehicles. Although we focus on applications to SSMs, our approach applies to the Likelihood-Free calibration of other models using multi-source data.

1. Introduction. Understanding individual-level consumer preferences is the basis of estimating and forecasting system-level demand in many applications in marketing and economics. Most individual-level behavioural models assume that the decision-makers are rational and choose an alternative with the highest utility. These models assume that decision-makers can process all available information and map it to the utility of each option before making a utility-maximizing choice. In the absence of data on decision-making processes, validating the assumptions of full information processing and utility-maximising behaviour is infeasible. For instance, these assumptions may not hold when decision-makers face realistic choice situations under time pressure, as they might not process all available information and deviate from utility-maximising decision rules (Caplin, 2016; Clithero, 2018).

With the advent of computer-based surveys and technological innovations, several types of process datasets can be collected, such as response time (i.e., the time elapsed from the

Keywords and phrases: Likelihood-Free Inference, Sequential Sampling Models, Multi-objective Bayesian Optimization.

presentation of alternative information to the confirmation of choice), mouse motion, and eye movements of the decision-maker (Bansal, Kim and Ozdemir, 2024). Some studies have explored the relationships between process datasets and choice outcomes. For instance, there is evidence of a speed-accuracy trade-off, where choice accuracy is inversely related to response time (Heitz, 2014), and a gaze-cascade effect, where decision-makers spend more time gazing at the chosen alternative before making a decision (Shimojo et al., 2003). These observations provide initial evidence that multi-source data on the decision-making process can enhance understanding of human decisions and offer better explanations of consumer preferences.

However, modelling multi-source data is challenging using the classic utility-based choice models as they are inherently static and do not have mechanisms to model the dynamic aspects of the decision-making process. Two potential approaches exist to model the decision-making process data with choice outcome data. First, a two-step choice model can be developed, such that the information searching process can be modelled using the decision-making process data in the first step, and choice outcome data can be used in the second step to explain the final decision conditional on the information processing (Gilbride and Allenby, 2004; Cheremukhin, Popova and Tutino, 2015). Second, Sequential Sampling Models (SSMs) from cognitive science provide a framework to utilize multi-source data to endogenously model the decision-making process and choice outcome (Smith, 2000). SSMs posit that the decision-maker gradually accumulates noisy information about available alternatives until the evidence reaches a certain threshold. The product with the highest positive evidence is chosen by the decision-maker. Neuroscientists also agree that the brain signals of decision-makers are compatible with the assumed decision-making process in SSMs (Pisauro et al., 2017). Based on the different structural formulations of the evidence accumulation process, several variants of SSMs have emerged, such as Multi-attribute Linear Ballistic Accumulator (MLBA, Trueblood, Brown and Heathcote, 2014) and Multi-alternative decision by sampling Model (MDbS, Noguchi and Stewart, 2018). While the two-step choice model is data-dependent and ad hoc, SSMs provide a generalizable framework to jointly model final choice (CH), response time (RT), and other process datasets.

Even though the framework and applications for SSMs are promising, their bottom-up design generally causes intractable joint likelihood of multi-source data, resulting in challenges associated with parameter estimation. As a compromise strategy, some researchers discretize RT into a few time steps to reduce computational burden (Noguchi and Stewart, 2018). Another strand of studies marginalizes the RT to only fit choice outcome data if the resulting likelihood has a closed-form expression (Ratcliff et al., 2016; Hancock, Hess and Choudhury, 2018), losing the core value of SSMs.

If computational issues are resolved, SSMs have the potential to become a workhorse model in marketing and economics to leverage decision-making process data in eliciting consumer preferences. In the absence of a closed-form likelihood for multi-source data, there is a need to develop a Likelihood-Free inference (LFI) approach to estimate SSMs that is computationally efficient and facilitates checks of consistency between different types of decision processes and choice data. LFI methods perform Bayesian inference using simulation of the model as a replacement for intractable likelihood evaluations. One of the most well-established LFI methods used in SSMs is approximate Bayesian computation (ABC, Sisson, Fan and Beaumont, 2018), which approximates the posterior by parameter samples for which a simulated dataset has a discrepancy from the observed dataset below a certain tolerance. See Section 2.1 for a more detailed discussion. ABC implicitly uses a kernel density approximation to the likelihood for data summaries. A competitive approach, probability density approximation (PDA, Turner and Sederberg, 2014), has also been widely used to estimate SSMs for over a decade. However, both ABC and PDA suffer from the curse of dimensionality, making them computationally intractable when the number of data summary statistics

is large, which is often required for highly parameterized models. Structured density estimation approaches which deal better with high-dimensional summary statistics include synthetic likelihood, which is based on a working normal model for summary statistics (Wood, 2010; Frazier et al., 2022), flexible extensions of synthetic likelihood based on copulas or empirical saddle point approximation (Fasiolo et al., 2018; An, Nott and Drovandi, 2020) and neural density estimation approaches (Papamakarios and Murray, 2016; Papamakarios, Sterratt and Murray, 2019; Greenberg, Nonnenmacher and Macke, 2019). Modern neural LFI methods have been used in the context of SSMs (e.g. Radev et al. (2023)) and for multi-source data (Schmitt, Radev and Bürkner, 2023). However, these structured density estimation methods require a large number of model simulations to obtain adequate approximations, which may be infeasible if simulation from the model is computationally expensive. A preferred approach in such settings is to use active learning approaches such as Bayesian optimization for Likelihood-Free inference (BOLFI, Gutmann and Corander, 2016), and extending these methods is the focus of our work. We review the BOLFI approach in Section 2.3, and related existing literature in Section A.2 of the Supplement. Our novel multi-objective extension of BOLFI (hereafter, MOBOLFI) shares the simulation efficiency of BOLFI but has key advantages compared to other Likelihood-Free approaches in handling intractable models for multi-source data. Crucially, our approach has the capability to approximate both the joint likelihood as well as likelihoods for individual data sources, enabling checks of the consistency of information supplied by different parts of the data. Examining this consistency is essential for trustworthy analysis of complex multi-source data such as those arising for SSMs. It is also valuable for understanding what data sources are most informative for the estimation of individual SSM parameters.

This work makes three main contributions. First, the multi-objective aspect of our MOBOLFI method ensures efficient exploration of the high-likelihood region for the separate likelihoods of all data sources. Second, the difficulty of combining multiple discrepancies from individual data sources into a single discrepancy - with the consequent information loss and highly conservative uncertainty quantification if poor choices are made - is avoided in the MOBOLFI approach, making it easier to use in practice. Finally, MOBOLFI is able to leverage likelihood approximations for individual data sources to check their consistency and understand their importance for estimating individual SSM parameters.

The paper is organized as follows. Section 2 gives background on Bayesian optimization and the BOLFI method of Gutmann and Corander (2016). Section 3 then discusses multi-objective optimization, the motivation for the MOBOLFI method, and its implementation. Section 4 presents two instructive examples, one involving a Brownian motion and the second involving a SSM. These examples illustrate the advantages of MOBOLFI compared to the BOLFI method with a single discrepancy in settings involving multi-source data. In the second example, we use an empirical choice-response time (choice-RT) dataset on consumer preferences for electric vehicles, and demonstrate MOBOLFI’s application in establishing the importance of different data sources for estimation of parameters of an SSM. Key takeaways and avenues for future research are discussed in section 5.

2. Method. Before explaining the MOBOLFI method, we give some necessary background on Bayesian optimization, ABC and the traditional BOLFI approach.

2.1. Approximate Bayesian computation. ABC methods are based on an approximation of the likelihood in terms of a synthetic dataset being close to the observed data according to some discrepancy. The discrepancy is often defined in terms of data summary statistics. It is important to explain the ABC likelihood approximation, since this motivates the BOLFI approach discussed in subsection 2.3. Interested readers will find a more extensive discussion of ABC than we give here in [Sisson, Fan and Beaumont \(2018\)](#).

Let θ be parameters in a statistical model for data $y \in \mathcal{Y}$ to be observed. Write y_{obs} for the observed value and $p(y_{\text{obs}}|\theta)$ for the likelihood, where $p(y|\theta)$ is the density of $y|\theta$. In ABC, inference is usually based on a lower-dimensional summary of the original data of dimension d say, defined by a mapping $S : \mathcal{Y} \rightarrow \mathbb{R}^d$. The observed summary statistic value $S(y_{\text{obs}})$ will be denoted by S_{obs} .

In ABC we first approximate the posterior density $p(\theta|y_{\text{obs}}) \propto p(\theta)p(y_{\text{obs}}|\theta)$ by the partial posterior density which conditions on S_{obs} rather than y_{obs} ,

$$p(\theta|S_{\text{obs}}) \propto p(\theta)p(S_{\text{obs}}|\theta).$$

If the summary statistics S are sufficient, then there is no loss in replacing y_{obs} with S_{obs} , but non-trivial sufficient statistics will not exist in most complex models of interest, and we only require summary statistics to be informative about θ . Next, since $p(S_{\text{obs}}|\theta)$ is infeasible to compute if $p(y_{\text{obs}}|\theta)$ is, we replace $p(S_{\text{obs}}|\theta)$ with the ‘‘ABC likelihood’’ denoted $p_t(S_{\text{obs}}|\theta)$ for some tolerance $t > 0$:

$$(2.1) \quad p_t(S_{\text{obs}}|\theta) \propto \int p(S|\theta)I(\Delta_\theta(S, S_{\text{obs}}) < t) dS,$$

where $\Delta_\theta(S, S_{\text{obs}}) = \|S - S_{\text{obs}}\|$ and $\|\cdot\|$ is some distance measure. $\Delta_\theta(S, S_{\text{obs}})$ is a measure of the discrepancy between the simulated and observed summary statistics. As discussed further below, the ABC likelihood at θ can be thought of as proportional to the probability that a synthetic dataset $S \sim p(S|\theta)$ is within t of the observed data in terms of the discrepancy. The ABC posterior is

$$(2.2) \quad p_t(\theta|S_{\text{obs}}) \propto p(\theta)p_t(S_{\text{obs}}|\theta),$$

and there are a variety of methods for sampling from (2.2), which are based on the fact that the right-hand side of (2.1) can be estimated unbiasedly by $I(\Delta_\theta(S, S_{\text{obs}}) < t)$ for $S \sim p(S|\theta)$. The discussion above can be generalized by replacing the indicator function with a more general kernel.

2.2. Bayesian optimization. Next we briefly describe Bayesian optimization (BO), which is used in the BOLFI method discussed in subsection 2.3. A more detailed introduction can be found in Garnett (2023). Bayesian optimization is used for finding a global optimum of a function $f(\theta)$, $\theta \in \Theta \subseteq \mathbb{R}^p$, where derivatives of $f(\cdot)$ are not available and evaluations of $f(\cdot)$ may be corrupted by noise. Here we consider minimization problems, but changing sign of the objective function turns minimization into maximization. BO models noisy evaluations of $f(\theta)$ with a surrogate model describing our uncertainty about $f(\cdot)$ given the function evaluations made so far. This surrogate model is usually chosen to be a Gaussian process (Rasmussen, 2003), and it guides the decision of where further function observations should be made.

Since the surrogate model we use for BO is a Gaussian process (GP), we need some background about GPs. A random function $f(\cdot)$ defined on Θ is a GP with mean function $\mu : \Theta \rightarrow \mathbb{R}$ and positive definite covariance function $C : \Theta \times \Theta \rightarrow \mathbb{R}$ if, for any n , and any $\theta_1, \dots, \theta_n \in \Theta$, the random vector $f(\theta_{1:n}) = (f(\theta_1), \dots, f(\theta_n))^\top$ is multivariate normally distributed, with mean vector $(\mu(\theta_1), \dots, \mu(\theta_n))$, and covariance matrix $C(\theta_{1:n}, \theta_{1:n}) = [C(\theta_i, \theta_j)]_{i,j=1}^n$. Suppose we observe the Gaussian process $f(\cdot)$ with noise at points $\theta_1, \dots, \theta_n \in \Theta$. The noisy observations are

$$(2.3) \quad z_i = f(\theta_i) + \epsilon_i, \quad i = 1, \dots, n,$$

where $\epsilon_i \stackrel{iid}{\sim} N(0, \sigma^2)$, for some variance $\sigma^2 > 0$. Write $z_{\leq n} = (z_1, \dots, z_n)^\top$. We are interested in describing uncertainty about $f(\theta^*)$ for some $\theta^* \in \Theta$, given the noisy observations $z_{\leq n}$. The distribution of $f(\theta^*)|z_{\leq n}$ is Gaussian, $N(\mu_n(\theta^*), \sigma_n^2(\theta^*))$, where the form of $\mu_n(\theta^*)$ and $\sigma_n^2(\theta^*)$ are given in Section A.1 in the Supplement.

The uncertainty quantification provided by the Gaussian process surrogate can be used to decide which θ^* should be used to obtain a further noisy observation

$$z^* = f(\theta^*) + \epsilon^*, \quad \epsilon^* \sim N(0, \sigma^2),$$

in our search for the minimizer of $f(\cdot)$. θ^* is usually chosen to minimize a so-called acquisition function. As an example, in the BOLFI method described next, [Gutmann and Corander \(2016\)](#) suggested using the lower confidence bound acquisition function ([Cox and John, 1997](#); [Srinivas et al., 2012](#)),

$$(2.4) \quad A_n(\theta) = \mu_n(\theta) - \sqrt{\eta_n^2 \sigma_n^2(\theta)}, \quad \text{where} \quad \eta_n^2 = 2 \log \left(n^{\frac{p}{2}+2} \frac{\pi^2}{3\epsilon_\eta} \right),$$

with the default value $\epsilon_\eta = 0.1$. Intuitively, $\mu_n(\theta)$ is an estimate of $f(\theta)$ from the noisy observations so far, and choosing θ^* to minimize $A_n(\theta)$ encourages choosing θ where this estimate is small, or where $\sigma_n^2(\theta)$ is large and we are highly uncertain about $f(\theta)$. Hence the Gaussian process model can help to manage an ‘‘exploration-exploitation trade-off’’ in searching for the minimum. Other acquisition functions can also be used ([Järvenpää et al., 2019](#)). Forms for the mean and covariance function need to be specified, and any parameters, including the noise σ^2 , estimated. This is usually done using marginal maximum likelihood.

2.3. BOLFI. We now discuss the use of Bayesian optimization in the BOLFI method of [Gutmann and Corander \(2016\)](#). A discussion of more recent work improving the BOLFI method is given in Section A.2 of the Supplement. We can rewrite the ABC likelihood (2.1) as

$$(2.5) \quad p_t(S_{\text{obs}}|\theta) \propto Pr(\Delta_\theta(S, S_{\text{obs}}) < t),$$

for $S \sim p(S|\theta)$. Hence the ABC likelihood can be approximated if we know the distribution of $\Delta_\theta(S, S_{\text{obs}})$, $S \sim p(S|\theta)$. This suggests we may be able to approximate the distribution of $\Delta_\theta(S, S_{\text{obs}})$ as a function of θ using regression, in order to obtain an approximation of the ABC likelihood. This is what the BOLFI method does, while using a sequential design approach based on BO to choose which θ to simulate from next for maximum benefit. The sequential design aspect allows simulation efficient exploration of the high likelihood region, making BOLFI highly suited for the case of computationally demanding simulation models.

[Gutmann and Corander \(2016\)](#) propose selecting parameter values for simulation using a BO algorithm to minimize the expected discrepancy function:

$$(2.6) \quad D(\theta) = E(\Delta_\theta(S, S_{\text{obs}})),$$

where the expectation is taken with respect to $S \sim p(S|\theta)$. In their approach, first some initial set of locations $\theta_i \in \Theta$, $i = 1, \dots, n_0$, are chosen according to some space-filling design. Synthetic data are then simulated at these locations to obtain discrepancy values $\Delta_i = \Delta_{\theta_i}(S_i, S_{\text{obs}})$, $S_i \sim p(S|\theta_i)$, $i = 1, \dots, n_0$. We can write

$$(2.7) \quad \Delta_i = D(\theta_i) + \epsilon_i, \quad i = 1, \dots, n_0,$$

where the ϵ_i are zero mean error terms. In BOLFI it is usually assumed, perhaps after a transformation of the Δ_i , that $\epsilon_i \sim N(0, \sigma^2)$ for some variance parameter σ^2 .

Next, model $D(\theta)$ as a Gaussian process, and denote the training data used to fit the Gaussian process model required for BO as $T_{n_0} = \{(\theta_i, \Delta_i) : i = 1, \dots, n_0\}$. A new location θ_{n_0+1} is then chosen to simulate the next summary statistic value and obtain the discrepancy Δ_{n_0+1} . This is done by optimization the BO acquisition function, which uses the uncertainties of the Gaussian process model to define the benefit of simulating a new discrepancy at any θ . The Gaussian process is then refitted with training data $T_{n_0+1} = T_{n_0} \cup \{(\theta_{n_0+1}, \Delta_{n_0+1})\}$.

The process of optimization of the acquisition function, simulation and retraining is repeated until some computational budget $n_f > n_0$ of simulations has been exhausted. The final Gaussian process model is then fitted to the training data T_{n_f} . Using the Gaussian process model and the noise assumption for (2.7), we can approximate the distribution of a discrepancy value observed at any θ . If we assume that $\Delta = D(\theta) + \epsilon$, and write $\mu_{n_f}(\theta), \sigma_{n_f}^2(\theta)$ for the mean and variance of the predictive distribution of $D(\theta)$ given T_{n_f} , then $D(\theta) \sim N(\mu_{n_f}(\theta), \sigma_{n_f}^2(\theta))$ and $\epsilon \sim N(0, \sigma^2)$ independently. We can approximate the distribution of Δ as $\Delta \sim N(\mu_{n_f}(\theta), \sigma_{n_f}^2(\theta) + \sigma^2)$. Further details about the derivation and form of $\mu_{n_f}(\theta)$ and $\sigma_{n_f}^2(\theta)$ are given in Section A.1 in the Supplement. Employing this Gaussian approximation to calculate the tail probability on the right-hand side of (2.5), we obtain

$$p_t(S_{\text{obs}}|\theta) \propto \Phi\left(\frac{t - \mu_{n_f}(\theta)}{\sqrt{\sigma_{n_f}^2(\theta) + \sigma^2}}\right),$$

where \propto denotes ‘‘approximately proportional to’’. This likelihood approximation can be used with MCMC sampling to draw approximate posterior samples from $p_t(\theta|S_{\text{obs}})$. The choice of tolerance t in our examples is discussed later.

3. The MOBOLFI method. Next we describe LFI with multi-source data with a discrepancy for each data source and the method of approximating the likelihood we consider. This is followed by background on multi-objective optimization, and finally the description of the new MOBOLFI method.

3.1. Likelihood approximation with multiple discrepancies. To ease notation, we consider the case of two data sources but the extension to three or more sources is immediate. Suppose the data y comprises $y = (x^\top, w^\top)^\top \in \mathcal{Y} = \mathcal{X} \times \mathcal{W}$ and decompose the joint density for $y|\theta$ as $p(y|\theta) = p(x|\theta)p(w|x, \theta)$. The observed data is $y_{\text{obs}} = (x_{\text{obs}}^\top, w_{\text{obs}}^\top)^\top$, the likelihood is $p(y_{\text{obs}}|\theta) = p(x_{\text{obs}}|\theta)p(w_{\text{obs}}|x_{\text{obs}}, \theta)$, and now there are summary statistics $S = (T^\top, U^\top)^\top : \mathcal{Y} \rightarrow \mathbb{R}^d$, where S concatenates summary statistic mappings T and U for the data sources x and w respectively, $T : \mathcal{X} \rightarrow \mathbb{R}^b$, $U : \mathcal{W} \rightarrow \mathbb{R}^c$, $d = b + c$. Write $S_{\text{obs}} = S(y_{\text{obs}})$, $T_{\text{obs}} = T(x_{\text{obs}})$ and $U_{\text{obs}} = U(w_{\text{obs}})$.

Similar to our previous discussion of ABC, we replace the likelihood $p(y_{\text{obs}}|\theta)$ with the summary statistic likelihood

$$(3.1) \quad p(S_{\text{obs}}|\theta) = p(T_{\text{obs}}, U_{\text{obs}}|\theta) = p(T_{\text{obs}}|\theta)p(U_{\text{obs}}|T_{\text{obs}}, \theta).$$

We then consider two discrepancies, $\Lambda_\theta(T, T_{\text{obs}})$ and $\Psi_\theta(U, U_{\text{obs}})$, for simulated summary statistic values $S = (T^\top, U^\top)^\top$, and formulate an ABC likelihood approximating (3.1) as

$$(3.2) \quad p_t(S_{\text{obs}}|\theta) \propto \int p(S|\theta)I(\Lambda_\theta(T, T_{\text{obs}}) < t_1)I(\Psi_\theta(U, U_{\text{obs}}) < t_2) dS,$$

where $t = (t_1, t_2)^\top$ is a discrepancy vector with $t_1, t_2 > 0$. Another way of writing (3.2) is

$$(3.3) \quad \begin{aligned} p_t(S_{\text{obs}}|\theta) &\propto P(\Lambda_\theta(T, T_{\text{obs}}) < t_1, \Psi_\theta(U, U_{\text{obs}}) < t_2) \\ &= P(\Lambda_\theta(T, T_{\text{obs}}) < t_1) \times P(\Psi_\theta(U, U_{\text{obs}}) < t_2 | \Lambda_\theta(T, T_{\text{obs}}) < t_1), \end{aligned}$$

for $S = (T^\top, U^\top)^\top \sim p(S|\theta)$.

The first term on the right-hand side of (3.3) approximates $p(T_{\text{obs}}|\theta)$, while the second approximates $p(U_{\text{obs}}|T_{\text{obs}}, \theta)$ (up to constants of proportionality). We could also approximate $P(U_{\text{obs}}|\theta)$ and $p(T_{\text{obs}}|U_{\text{obs}}, \theta)$ by switching the two discrepancies in (3.3). Our extension of BOLFI will model $\Delta_\theta(S, S_{\text{obs}})$ for $S \sim p(S|\theta)$ as a bivariate Gaussian process. We will use this bivariate process for sequential design using multi-objective Bayesian optimization, and also for approximation of data-source specific likelihood contributions such as those shown in (3.3).

3.2. *Multi-objective optimization.* Our MOBOLFI extension of BOLFI uses multi-objective optimization, and we describe this now. Let $f(\theta) = (f_1(\theta), \dots, f_K(\theta))^\top$ be a multivariate function, and suppose we wish to minimize the components of $f(\cdot)$. There need not be any common $\theta^* \in \Theta$ for all components where a minimum is achieved, and multi-objective optimization methods approximate the set of “nondominated” solutions which are not obviously inferior to any other solution. We say that a value $\theta \in \Theta$ dominates $\theta' \in \Theta$ if $f_j(\theta) \leq f_j(\theta')$, $j = 1, \dots, K$, with the inequality being strict for at least one j . The dominated solution is inferior for minimizing $f(\cdot)$ along some dimensions and no better for other dimensions. Multi-objective optimization algorithms try to find the set of nondominated points in Θ , the “Pareto optimal set”.

The Pareto optimal set is infinite in general, and numerical multi-objective optimization methods obtain finite approximations to it. The Pareto set is mapped by $f(\cdot)$ onto the Pareto frontier, the set of optimal function values obtained by the points in the Pareto set. Multi-objective Bayesian optimization (Garnett, 2023, Section 11.7) uses surrogate models to implement multi-objective optimization for expensive to evaluate functions, possibly observed with noise. Similar to Bayesian optimization with a scalar objective, the representation of uncertainty given by the surrogate is used to efficiently decide where to perform the next function evaluation.

The surrogate model in our work is a multivariate Gaussian process, and we need to explain what this means. Let $f(\theta) = (f_1(\theta), \dots, f_K(\theta))^\top$, $\theta \in \Theta$, be a multivariate random function. It is a multivariate Gaussian process with mean function $\mu : \Theta \rightarrow \mathbb{R}^K$, $\mu(\theta) = (\mu_1(\theta), \dots, \mu_K(\theta))^\top$, and positive definite covariance function $C : \Theta \times \Theta \rightarrow \mathbb{R}^{K \times K}$, if for any n , and $\theta_1, \dots, \theta_n \in \Theta$, $f(\theta_{1:n}) = (f(\theta_1)^\top, \dots, f(\theta_n)^\top)^\top$ is multivariate Gaussian with mean $\mu(\theta_{1:n}) = (\mu(\theta_1)^\top, \dots, \mu(\theta_n)^\top)^\top$, and covariance matrix $C(\theta_{1:n}, \theta_{1:n}) = [C(\theta_i, \theta_j)]_{i,j=1}^n$, with $K \times K$ block elements $C(\theta_i, \theta_j)$. Once again extending the discussion of subsection 2.2, suppose we observe values of $f(\cdot)$ with noise at $\theta_1, \dots, \theta_n \in \Theta$, to obtain

$$(3.4) \quad z_i = f(\theta_i) + \epsilon_i,$$

where now $z_i \in \mathbb{R}^K$ and $\epsilon_i \stackrel{iid}{\sim} N(0, \Sigma)$ where $\Sigma \in \mathbb{R}^{K \times K}$ is some positive definite covariance matrix. For any $\theta^* \in \Theta$, and writing $z_{\leq n} = (z_1^\top, \dots, z_n^\top)^\top$, The distribution of $f(\theta^*) | z_{\leq n}$ is multivariate Gaussian, $N(\mu_n(\theta^*), \Sigma_n(\theta^*))$, where the form of $\mu_n(\theta^*)$ and $\Sigma_n(\theta^*)$ are given in Section A.3 in the Supplement. Given the uncertainty quantification provided by the multivariate Gaussian surrogate, an acquisition function can be defined. If there is a finite set of points, say $\theta_1, \dots, \theta_n$, approximating the Pareto set, with corresponding approximation f_1, \dots, f_n of the Pareto frontier, one measure of performance that has been used is the volume of the space dominated by the current approximation of the Pareto frontier and bounded below by a reference point, the so-called Pareto hypervolume. Expected hypervolume improvement (EHVI) was first used as an acquisition function in multi-objective Bayesian optimization by Emmerich (2005). For implementing the MOBOLFI method of the next section, we use the noisy expected hypervolume improvement (NEHVI) method of Daulton, Balandat and Bakshy (2021a) which copes well with noisy function evaluations and the trialing of batches of solutions in parallel with reduced computational demands. The method is implemented in the open source python package `BoTorch` (Balandat et al., 2020). We will not discuss further the extensive literature on multi-objective Bayesian optimization, but refer the reader to Garnett (2023, Section 11.7) for an accessible introduction.

3.3. *MOBOLFI.* While BOLFI provides a closed form approximate likelihood for inference tasks, it cannot approximate likelihoods for individual data sources for multi-source

data. Multi-source data has become increasingly common in SSM design in recent years. Often it is natural to choose summary statistics and discrepancy metrics separately for each data source, and with the classic BOLFI approach we then need to combine all discrepancies into a single one. If this is not done carefully, the information in the combined discrepancy may not reflect correctly the relative importance of different data sources, resulting in information loss and highly conservative uncertainty quantification.

Motivated by these issues for multi-source data, we develop our MOBOLFI extension of the original BOLFI method. It achieves simulation efficient likelihood approximations in LFI for multi-source data by applying multi-objective BO methods to a vector of data-source specific discrepancy functions. Consider again the bivariate setting and notation of subsection 3.1 for simplicity, and define the vector of expected discrepancies

$$D(\theta) = E(\Delta_\theta(S, S_{\text{obs}})) = (D_1(\theta), D_2(\theta))^\top,$$

where $D_1(\theta) = E(\Lambda_\theta(T, T_{\text{obs}}))$, $D_2(\theta) = E(\Psi_\theta(U, U_{\text{obs}}))$, $S = (T, U) \sim p(S|\theta)$. A multi-objective Bayesian optimization algorithm applied to $D(\theta)$ efficiently explores the set of θ where both of the data source discrepancy components is likely to be small, leading to efficient approximations to the likelihood contributions from multiple data sources.

The optimization algorithm proceeds similarly to the case of a univariate objective. Firstly, we choose some initial set of points $\theta_1, \dots, \theta_n \in \Theta$ according to some space filling design. We then simulate discrepancy values $\Delta_i = \Delta_{\theta_i}(S_i, S_{\text{obs}})$, $S_i \sim p(S|\theta_i)$, $i = 1, \dots, n_0$, and we can write

$$(3.5) \quad \Delta_i = D(\theta_i) + \epsilon_i,$$

where the ϵ_i are zero mean independent errors. It will be assumed that $\epsilon_i \sim N(0, \Sigma)$, for some covariance matrix Σ . Assuming a Gaussian process model for $D(\cdot)$, we fit a Gaussian process surrogate model to the training data $T_{n_0} = \{(\theta_i, \Delta_i) : i = 1, \dots, n_0\}$, learning all hyperparameters including Σ from the data. We can then choose the next observation point θ_{n_0+1} to minimize the NEHVI acquisition function (or perhaps choose a batch of points), retrain the GP and acquire new points, continuing until we have n_f training points for the final fitted GP. In GP fitting, we use a constant mean function and Matérn covariance kernel.

From the model (3.5) and the assumed $N(0, \Sigma)$ distribution of the errors, we can approximate the ABC likelihood (3.3) up to a proportionality constant by a bivariate Gaussian probability given a well-chosen vector-valued tolerance $t = (t_1, t_2)$:

$$(3.6) \quad \tilde{p}_t(S_{\text{obs}}|\theta) := \Phi((t_1, t_2); \mu_{n_f}(\theta), \Sigma_{n_f}(\theta) + \Sigma),$$

where $\Phi(\cdot; \mu_{n_f}(\theta), \Sigma_{n_f}(\theta))$ denotes the cdf of a normal $N(\mu_{n_f}(\theta), \Sigma_{n_f}(\theta) + \Sigma)$ distribution. Henceforth we will omit the ‘‘up to a proportionality constant’’ qualification when we talk about likelihood approximations. It is also possible to decompose the bivariate probability (3.6) into marginal and conditional components, approximating the terms $P(\Lambda_\theta(T, T_{\text{obs}}) < t_1)$ and $P(\Psi_\theta(U, U_{\text{obs}}) < t_2 | \Lambda_\theta(T, T_{\text{obs}}) < t_1)$ which in turn approximate $p(T_{\text{obs}}|\theta)$ and $p(U_{\text{obs}}|T_{\text{obs}}, \theta)$. The discrepancies can also be swapped in the above expressions. Write $\mu_n(\theta) = (\mu_{n1}(\theta), \mu_{n2}(\theta))^\top$, and write $\Sigma_{nij}(\theta)$ and Σ_{ij} for the (i, j) th entries of $\Sigma_n(\theta)$ and Σ respectively, $j = 1, 2$. We approximate $p(T_{\text{obs}}|\theta)$ by

$$(3.7) \quad \tilde{p}_t(T_{\text{obs}}|\theta) := \Phi\left(\frac{t_1 - \mu_{n1}(\theta)}{\sqrt{\Sigma_{n11}(\theta) + \Sigma_{11}}}\right),$$

and $p(U_{\text{obs}}|T_{\text{obs}}, \theta)$ by

$$(3.8) \quad \tilde{p}_t(U_{\text{obs}}|T_{\text{obs}}, \theta) := \Phi\left(\frac{t_2 - \mu_{n2|1}(\theta)}{\sqrt{\Sigma_{n2|1}(\theta)}}\right),$$

where

$$\mu_{n2|1}(\theta) = \mu_{n2}(\theta) + \frac{\Sigma_{n12}(\theta) + \Sigma_{12}}{\Sigma_{n22}(\theta) + \Sigma_{22}}(T_{\text{obs}} - \mu_{n1}(\theta)),$$

and

$$\Sigma_{n2|1}(\theta) = \Sigma_{n22}(\theta) + \frac{(\Sigma_{n12}(\theta) + \Sigma_{12})^2}{\Sigma_{n22}(\theta) + \Sigma_{22}}.$$

The likelihood for $p(U_{\text{obs}}|\theta)$ can be approximated by

$$(3.9) \quad \tilde{p}_t(U_{\text{obs}}|\theta) := \Phi\left(\frac{t_2 - \mu_{n2}(\theta)}{\sqrt{\Sigma_{n22}(\theta) + \Sigma_{22}}}\right).$$

Gutmann and Corander (2016) chose the tolerance t in the univariate BOLFI method as the q -quantile of $\Delta_1, \dots, \Delta_{n_f}$, where $q \in (0, 1)$. In the bivariate MOBOLFI method, we extend the choice of tolerance $t = (t_1, t_2)$ to the 2-dimensional vector q -quantile of $\Delta_1, \dots, \Delta_{n_f}$, where $q \in (0, 1)^2$. The approximate likelihood (3.6) is sensitive to the value of t . For results in this paper, we set the $q = 0.05$. A comparison study over different q -quantile tolerance is given in for 3 different examples in the Supplement. The dependent noise covariance matrix Σ is estimated by the covariance of a repeatedly simulated sample $\{\Delta_{i_\Sigma, j}\}_{j=1}^{n_\Sigma}$, where $\Delta_{i_\Sigma, j} = D(\theta_{i_\Sigma}) + \epsilon_{i_\Sigma}$ are simulated noisy discrepancies for some θ_{i_Σ} . For results in this paper, we set $n_\Sigma = 100$ and $\theta_{i_\Sigma} = \arg \min_{(\theta_i, \Delta_i) \in T_{n_f}} (\Delta_i - \mu_{n_f}(\theta_i))^\top \Sigma_{n_f}(\theta_i)^{-1} (\Delta_i - \mu_{n_f}(\theta_i))$.

better performance and numerical stability, we apply scaling to control the magnitude of Δ . Details of scaling are provided in Section A.3 of the Supplement.

3.4. *Checking consistency of different data sources.* There are a number of advantages in separately approximating likelihood contributions in a problem with multi-source data. One of the most important is the ability to detect conflicting information about the parameter from different parts of the data. Given a prior $p(\theta)$ we can use the likelihood approximation (3.6) to sample from the approximate posterior

$$(3.10) \quad \tilde{p}_t(\theta|S_{\text{obs}}) \propto p(\theta)\tilde{p}_t(S_{\text{obs}}|\theta).$$

Using MCMC to sample from this does not involve any further (computationally expensive) simulation from the model. This is true for the other posterior approximations discussed below also. If the two components of the likelihood are in conflict and induce modes in different regions of the parameter space, our method of multivariate approximation can capture some of that complexity by separately considering the likelihood contributions for the different data sources.

If we want to know what information is contained in the first data source only, we can compute the approximate posterior

$$(3.11) \quad \tilde{p}_t(\theta|T_{\text{obs}}) \propto p(\theta)\tilde{p}_t(T_{\text{obs}}|\theta).$$

Comparing the posterior densities (3.10) and (3.11) tells us how the second data source changes the inference. We could also consider a weakly informative prior $p_W(\theta)$ and consider the information about the parameter contained in each data source through the posterior approximations

$$(3.12) \quad \tilde{p}_t(\theta|T_{\text{obs}}) \propto p_W(\theta)\tilde{p}_t(T_{\text{obs}}|\theta)$$

and

$$(3.13) \quad \tilde{p}_t(\theta|U_{\text{obs}}) \propto p_W(\theta)\tilde{p}_t(U_{\text{obs}}|\theta).$$

The purpose of using a weakly informative prior here is to separate the information in the data from that contained in the prior, in so far as that is possible.

In this work we consider only informal comparisons of posteriors based on different data and prior choices, but there are more formal methods to check for conflict between priors and data, or more generally between information in different parts of a hierarchical model. We refer the reader to [Evans and Moshonov \(2006\)](#), [Marshall and Spiegelhalter \(2007\)](#) and [Presanis et al. \(2013\)](#) for further discussion of these.

4. Examples. In this section, we implement MOBOLFI in several examples. First, we apply MOBOLFI to a simple synthetic data example where we can illustrate the advantages of MOBOLFI compared to BOLFI for multi-source data, including the situation where misspecification is present. Following this, we use MOBOLFI to estimate a sequential sampling model (SSM), the Multi-attribute Linear Ballistic Accumulator (MLBA), to highlight MOBOLFI’s superior design for choice-RT joint data sources compared to BOLFI. MLBA is chosen from other SSMs because of its generality for diverse choice situations and its closed-form likelihood, which enables gold-standard comparisons to be made for the likelihood approximations used in MOBOLFI. MOBOLFI requires training a bivariate GP, which involves higher computational cost than the BOLFI training of a univariate GP. However, if model simulation is computationally expensive, this will dominate the computation time for both methods. Although the likelihood is tractable for the MLBA model, summary statistic based Likelihood-Free inference can be of interest when the assumed model is misspecified. In this case, conditioning on insufficient statistics that discard information which cannot be matched by the assumed model while matching important features can be used to develop models that are “fit for purpose” - see for example [Lewis, MacEachern and Lee \(2021\)](#) for further discussion.

The detailed setup of our experiments and further analyses are described in Sections B and C of the Supplement. Section D in the Supplement discusses an example on bacterial transmission in day care centres ([Gutmann and Corander, 2016](#); [Numminen et al., 2013](#)). Codes and detailed results are submitted to github: <https://github.com/DZCQs/Multi-objective-Bayesian-Optimization-Likelihood-Free-Inference-MOBOLFI.git>.

4.1. Toy example. Our first synthetic example uses the MOBOLFI method to infer a parameter $\theta = (\theta_1, \dots, \theta_{10})^\top \in \mathbb{R}^{10}$ for a model with two data sources. The example is modified from [Schmitt, Radev and Bürkner \(2023\)](#). The first data source consists of $N = 20$ independent 10-dimensional normal observations with mean θ , $X_n \sim N(\theta, I)$, $n = 1, \dots, N$. The second data source consists of $M = 50$ 10-dimensional observations W_m , $m = 1, \dots, 50$. The W_m are obtained by observing discretely the following ten-dimensional Brownian motion (BM) with drift:

$$dw(t) = \theta dt + \sigma dW(t), \quad t \in [0, 3],$$

where $w(0)$ is a ten-dimensional vector of zeros, $W(t)$ is a standard ten-dimensional BM, and $\sigma = 0.5$, leading to $W_m = w((m-1)\delta)$, $\delta = 3/(M-1)$, $m = 1, \dots, M$.

For the dataset $X = \{X_n\}_{n=1}^N$, and corresponding observed data denoted $\{X_n^o\}_{n=1}^N$, we write $\bar{X} = N^{-1} \sum_n X_n$, $\bar{X}^o = N^{-1} \sum_n X_n^o$ and the discrepancy for data source X is $\Delta_1(X, X^o) = \|\bar{X} - \bar{X}^o\|$, where $\|\cdot\|$ denotes the Euclidean distance. For data $W = \{W_m\}_{m=1}^M$, and observed data $W^o = \{W_m^o\}_{m=1}^M$, we write $\Delta W_m = Y_{m+1} - W_m$, $m = 1, \dots, M-1$, $\Delta W_m^o = W_{m+1}^o - W_m^o$, $m = 1, \dots, M-1$, $\bar{\Delta W} = (M-1)^{-1} \sum_{m=1}^{M-1} \Delta W_m$ and $\bar{\Delta W}^o = (M-1)^{-1} \sum_{m=1}^{M-1} \Delta W_m^o$. Then the discrepancy used for data source Y is $\Delta_2(W, W^o) = \|\bar{\Delta W} - \bar{\Delta W}^o\|$.

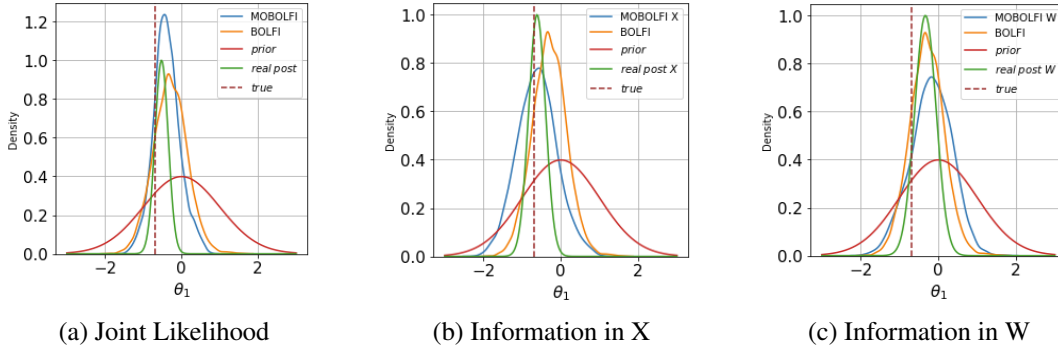


Figure 1: Approximate posteriors for the toy example. The left column shows approximate posteriors for the joint likelihood. The middle/right columns show approximate posteriors conditioning only on X/W . The blue and orange curves are kernel density estimates obtained from HMC samples for MOBOLFI and BOLFI posteriors respectively. The green curves shows the true posteriors (joint/ X/W on left/middle/right column respectively), and the red dash line is $\theta_1^{\text{true}} = -0.7$.

We generate the observed data (X^o, W^o) for the analysis by simulation with $\theta^{\text{true}} = (-0.7, 0.7, \dots, -0.7, 0.7)^T$. For implementing BOLFI and MOBOLFI, 100 initial prior samples $\{\theta^{(i)}, (X^{(i)}, W^{(i)})\}_{i=1}^{100}$ are drawn, where $X^{(i)} = \{X_n^{(i)}\}_{n=1}^N$, $W^{(i)} = \{W_m^{(i)}\}_{m=1}^M$, $\theta^{(i)} \sim N(0, I)$, and $X^{(i)}$ and $W^{(i)}$ are the i th simulations for X and W given $\theta^{(i)}$. The training data is $\{\theta^{(i)}, (\Delta_1(X^{(i)}, X^o), \Delta_2(W^{(i)}, W^o))\}_{i=1}^{100}$. For implementing the BOLFI approach, we get a single discrepancy by a weighted sum of the two data source specific discrepancies, $0.4\Delta_1(X, X^o) + \Delta_2(W, W^o)$. The weight of 0.4 on the first discrepancy is chosen to put the two data source specific discrepancies on a similar scale. For implementing MOBOLFI, we use the vector discrepancy (Δ_1, Δ_2) . For both approaches, 150 acquisitions are made in the BO algorithm, and 250 model simulations are needed in total.

Given the symmetry of the model in the way that the components of θ , X and W are generated, without loss of generality we present only results for inference about θ_1 . Figure 1 compares MOBOLFI and BOLFI approximate posteriors of θ_1 . We make three observations. First, in the left column of the figure, Hamiltonian Monte Carlo (HMC) samples from the MOBOLFI approximate posterior exhibit lower variance compared to those from the BOLFI posterior, and the MOBOLFI posterior is closer to the true posterior. This suggests that there is information loss using a single discrepancy compared to MOBOLFI with multiple discrepancies unless the combination of data-source specific discrepancies is done very carefully. Second, the true posterior has smaller variance than the approximate posteriors. This is expected and mostly reflects the finite tolerance used and uncertainty in the likelihood approximation from the surrogate model. Third, the MOBOLFI approximations to the posterior conditional on X or W only show similar posterior location to the corresponding true posteriors, but with somewhat larger variance. The MOBOLFI posteriors conditional on individual data sources are obtained without significant additional computation after the posterior approximation for the joint posterior has been obtained. Additional findings are described in Section B.2 of the Supplement, where we explore the effect of tolerance and the number of BO acquisitions on the inference. An additional experiment is described there that investigates whether the performance of MOBOLFI is affected when some parameters are present in only a subset of the data source-specific models.

4.1.1. *Misspecified simulator.* We continue the above example by modifying it to introduce misspecification. Our purpose is to demonstrate that MOBOLFI is useful for under-

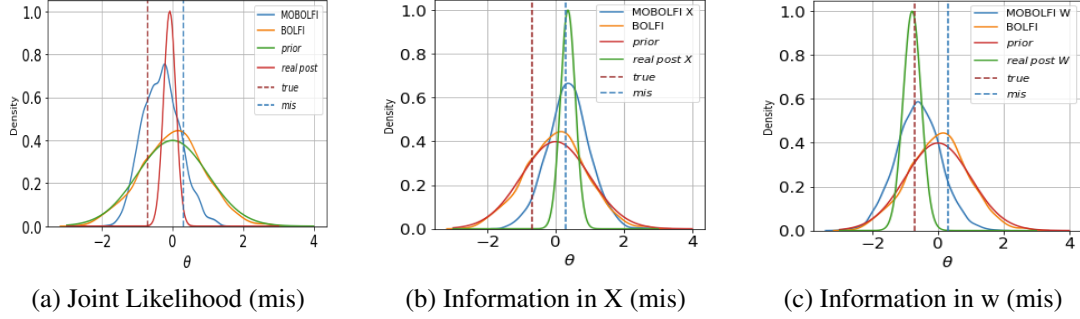


Figure 2: Approximate posteriors for the toy example under misspecification. The left column shows MOBOLFI and BOLFI approximate posterior densities conditional on both X and W . The middle/right presents approximate posterior densities conditioning only on X/W . The blue and orange curves are kernel estimates of posterior densities from HMC samples for MOBOLFI and BOLFI respectively. The green curve shows the true posterior (joint/ X/W on left/middle/right column respectively). The two red dash lines are $\theta_X = 0.3$ and $\theta_W = -0.7$.

standing misspecification when different data sources provide conflicting information. In the modified example the observations are one-dimensional, $X_n \sim N(\theta, 1)$, $n = 1, \dots, N$, and W_m , $m = 1, \dots, M$, with $W_m = w((m-1)\delta)$, $\delta = 3/(M-1)$ with $w(t)$, $t \in [0, 3]$ a univariate process defined by

$$dw(t) = \theta dt + \sigma dW(t), \quad w(0) = 0,$$

with $W(t)$ a univariate standard BM, and N , M and σ as before.

The true data generating process (DGP) is not the above assumed model. Instead, in the true DGP there are different values of θ in the models for X and W , so that $X_n \sim N(\theta_X, 1)$ and $dw(t) = \theta_W dt + \sigma dW(t)$, where $\theta_X \neq \theta_W$. We simulate the observed data for the analysis using $\theta_X = 0.3$, $\theta_W = -0.7$. In the misspecified assumed model the likelihood contributions for different data sources produce conflicting information about θ .

Approximate posteriors for θ are presented in Figure 2. The MOBOLFI and BOLFI approximate posteriors are similar when conditioning on both X and W , with the posterior mode lying between θ_X and θ_W . The middle/right columns shows the MOBOLFI approximate posterior conditioning on only X , or only Y , compared to the corresponding true posterior and the BOLFI posterior conditioning on both X and Y . We make two observations. First, the MOBOLFI approximate posteriors conditioning on X only and on Y only produce good estimates of θ_X and θ_W , and the conflicting information in the two data sources is evident. Second, the approximations of the individual data source posteriors in MOBOLFI are obtained without substantial additional computation, since the joint likelihood and likelihoods for X and Y are obtained simultaneously in the MOBOLFI approach.

4.2. Multi-attribute Linear Ballistic Accumulator. MLBA is a state-of-the-art SSM for understanding the human decision-making process. We will apply MOBOLFI to infer parameters of one variant of MLBA (Hancock et al., 2021a) using a simulated dataset where θ is known, and for a real-world dataset on preferences of ridehailing drivers to rent electric vehicles in Singapore.

4.2.1. Simulator introduction. MLBA assumes that decision-making can be seen as an evidence accumulation process, as illustrated in Figure 3. For a decision-maker facing M alternatives, MLBA posits there exist M independent evidence accumulators starting to

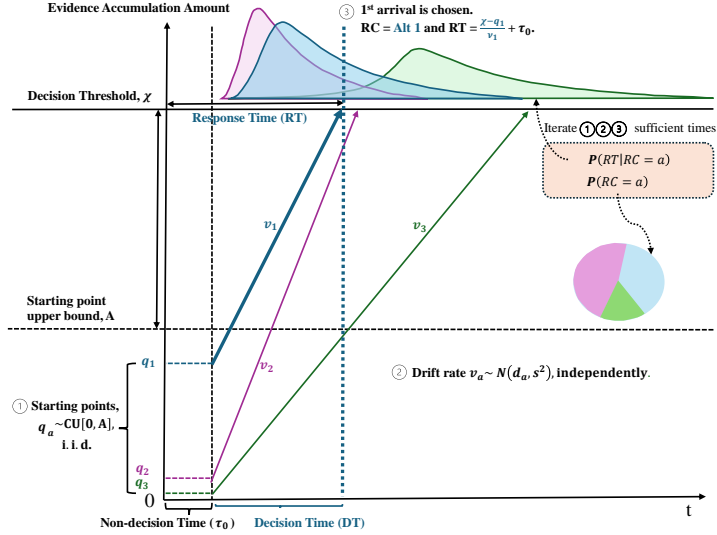


Figure 3: The simulation process of MLBA for three alternatives ($M = 3$). In this case, the final choice outcome is Alternative 1 (in blue and its accumulator is bold). The RT is the time for Alternative 1 to reach the threshold with non-decision time τ_0 . The directed solid lines demonstrate the realized evidence accumulation trajectory for each alternative. The MLBA simulator contains three steps annotated above. After iterating sufficient times, the choice proportion and its conditional RT distribution can be acquired.

collect supporting evidence for each corresponding alternative a from a random starting point $q_a \stackrel{i.i.d.}{\sim} \mathcal{U}[0, A]$. Each alternative-specific accumulator evolves linearly at drift rate $v_a \stackrel{indep.}{\sim} N(d_a, s^2)$, where $a = 1, \dots, M$. d_a depends on the pairwise attribute comparisons for all K attributes of alternative a with the remaining alternatives for each observation. A and s^2 are constant over observations to measure the scale of initial preference and unobserved accumulation process noise, respectively. Finally, the alternative whose evidence accumulator reaches the common threshold χ first is considered the final choice, and the deliberation time is the same as this alternative's evidence accumulation time $\frac{\chi - q}{v}$. Strictly, the response time (RT) is defined as the sum of the deliberation time and the non-decision time, which stands for information encoding and decision execution time. However, for complex choice tasks with multi-attribute information, non-decision time can be omitted if it does not contribute significantly to RT.

The MLBA model can be described in two parts. The *back-end part*, Linear Ballistic Accumulator (LBA), was originally proposed by [Brown and Heathcote \(2008\)](#) for implicit choice situations (i.e., choice tasks without listed attribute values). To extend LBA to MLBA, [Trueblood, Brown and Heathcote \(2014\)](#) added the *front-end part* to LBA by specifying alternative-specific drift rates. Several variants of the front-end part have been investigated to define the drift rate mean of MLBA. We choose [Hancock et al. \(2021a\)](#)'s specification because it can handle more than two attributes. For a choice set \mathcal{C} , the drift rate mean d_a for the alternative a is:

$$(4.1) \quad d_a = \max\{I_0 + \delta_a + \sum_{b \in \mathcal{C}, b \neq a} \sum_{k=1}^K \omega_{abk} \beta_k (X_{ak} - X_{bk}), 0\},$$

where X_{ak} is the value of attribute k of alternative a and

$$(4.2) \quad \omega_{abk} = \begin{cases} \exp\{-\lambda_1|\beta_k(X_{ak} - X_{bk})|\} & \beta_k(X_{ak} - X_{bk}) \geq 0 \\ \exp\{-\lambda_2|\beta_k(X_{ak} - X_{bk})|\} & \beta_k(X_{ak} - X_{bk}) < 0. \end{cases}$$

The final simulation output is a concatenation of RT and choice outcome:

$$(4.3) \quad (RT, CH) = ((\chi - g_{CH})/v_{CH}) + \tau_0, \underset{a \in \mathcal{C}}{\operatorname{argmin}}(\chi - g_a)/v_a)$$

$\Lambda := (\lambda_1, \lambda_2)$ is interpreted as a vector of sensitivity parameters of positive/negative difference of attribute pairwise-comparisons respectively; I_0 is a common drift rate mean constant that prevents negative drift rate; $\beta = (\beta_1, \dots, \beta_K)$ are scaling parameters for the attributes; and $\delta = (\delta_1, \dots, \delta_M)$ are alternative-specific constants for the drift rate mean. Thus, the estimable parameter is $\theta = (\Lambda, I_0, \beta, \delta_{-1}, \chi)$, while $(\mathcal{A}, s, \tau_0, \delta_1)$ are fixed for parameter identification and $\delta_{-1} = (\delta_2, \dots, \delta_M)^T$. Following [Brown and Heathcote \(2008\)](#) and [Terry et al. \(2015\)](#), the joint likelihood of observing the response time RT and the choice made CH of multiple candidates has a closed form expression. It is presented in Section C.1 of the Supplement. We use the closed-form likelihood as a gold-standard to benchmark approximate posteriors obtained by LFI in subsequent experiments.

4.2.2. Synthetic data. We use the survey question design and alternative-specific attribute matrix for the real example of section 4.2.3. A choice question with $M = 3$ alternatives is provided to candidates. Each alternative offers values of $K = 3$ attributes, and a respondent will make decisions by evaluating the alternative and its attributes. For data generation, the synthetic output data is simulated using $\theta = (\Lambda, I_0, \beta, \delta, \chi) = ((0.1, 0.8), 2, (-22, -5, -6), (0, 3, 1.5), 100)$, resulting in $1280 = 320 \cdot (3 + 1)$ observations, after concatenating CH (in one-hot encoding) and RT for 320 candidates. The size of the alternative-specific attribute matrix X is 320×9 . For parameter estimation, the true values of parameters we target in inference are $\theta^{\text{true}} = (\lambda_1, \beta_1, \beta_2, \delta_2, \delta_3, \log(\chi - \mathcal{A}))^{\text{true}} = (0.1, -5, -6, 3, 1.5, \log(99))$. The parameters $\mathcal{A}, s, \tau_0, \delta_1$ are fixed at 1, 1, 0, and 0 for identifiability, and $\lambda_2 = 0.8, I_0 = 2, \beta_3 = -6$ are assumed to be known for reducing the computational cost in further training such as facilitating scaling of the estimable parameters. This implementation is common in empirical studies since MLBA is designed bottom-up so that some parameters are highly correlated with each other. Lastly, we have log-transformed $\chi - \mathcal{A}$ in order to increase sampling efficiency, since the magnitude of $\log(\chi - \mathcal{A})$ is much smaller than that of χ .

The synthetic data (RT^o, CH^o) is simulated by MLBA taking θ^{true} as input, where RT and CH are response time and choices. For implementing BOLFI and MOBOLFI, 100 samples from the prior are used as initialization, $\{\theta^{(i)}, (RT^{(i)}, CH^{(i)})\}_{i=1}^{100}$, where $RT^{(i)} = \{RT_1^{(i)}, \dots, RT_{320}^{(i)}\}$, and $CH^{(i)} = \{CH_1^{(i)}, \dots, CH_{320}^{(i)}\}$ are the simulated data given $\theta^{(i)}$. For response times RT , write \widetilde{RT} for the vector of order statistics of RT . Similarly, \widetilde{RT}^0 is the vector of order statistics of RT^0 . The training data is $\{\theta^{(i)}, (\Delta_1(RT^{(i)}, RT^o), \Delta_2(CH^{(i)}, CH^o))\}_{i=1}^{100}$, where $\Delta_1(RT, RT^o)$ and $\Delta_2(CH, CH^o)$ are discrepancies for the response and choice data respectively. The first discrepancy is defined as

$$(4.4) \quad \Delta_1(RT, RT^o) = \|\log(\widetilde{RT}^0) - \log(\widetilde{RT})\|_1,$$

where $\|\cdot\|_1$ denotes the L_1 distance. For the second discrepancy, recall that the CH data is represented by 3 dimensional one-hot encoding of 3 alternatives, and we define

$$(4.5) \quad \Delta_2(CH^{(i)}, CH^o) = \frac{1}{3} \left\| \frac{1}{320} \sum_{j=1}^{320} |CH_j^o - CH_j^{(i)}| \right\|_1.$$

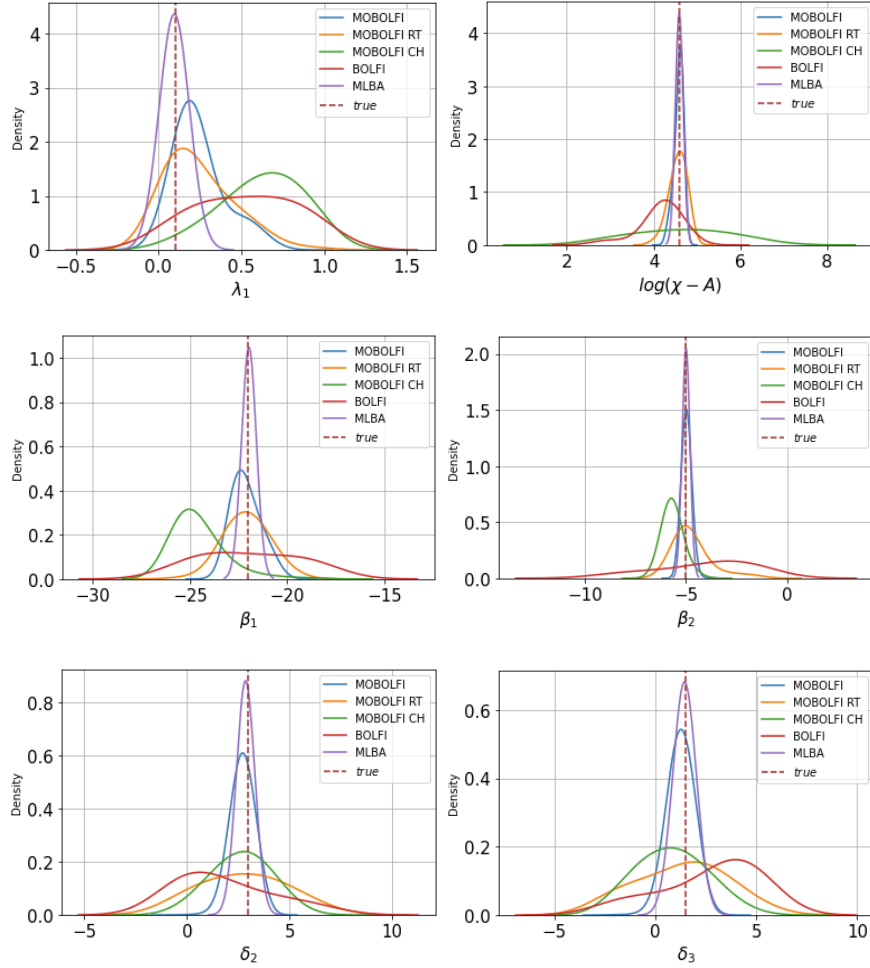


Figure 4: Approximate posteriors for MLBA example. The plots shows marginal posteriors for different methods and each parameter of interest. The blue/red curve represents the MOBOLFI approximate posterior/BOLFI approximate posterior. The purple curve is the sample from the closed form posterior¹, calculated using the closed form likelihood of MLBA. The orange/green curves are the MOBOLFI approximate posteriors calculated by marginal approximate likelihood of *RT/CH* data. The red dashed line is the value of θ^{true} .

The prior assumes independence between components of θ , with each marginal prior uniform on an interval of length 8 centred on the true value, with the exception of the parameter λ which has a prior uniform on $[0, 1]$. Differential emission MCMC (De-MCMC, [Turner et al. \(2013\)](#)) is used to sample from the approximate posterior. Further details of the experiment are given in Section C.2 of the Supplement.

Figure 4 shows approximate posterior distributions obtained using the BOLFI and MOBOLFI methods. We make a number of observations. First, the variance of the MOBOLFI approximate posterior is smaller than that for BOLFI. In fact, MOBOLFI using only the response time data produces more accurate approximations of the true posterior than BOLFI given both data sources. This suggests that when it is natural to define discrepancies separately for different data sources, combining them linearly, even with weights, may result in information loss. Second, both MOBOLFI and BOLFI posterior variances are larger than for the true posterior, which is expected, due to the irreducible information loss from ap-

proximation. Third, when comparing the MOBOLFI posteriors calculated by likelihoods of different data sources, the posterior using both data sources is better than any posterior using only one data source. Fourth, for inference of β and λ_1 , the posterior using only CH has its marginal maximum a posteriori probability (MAP) value far from the value of θ^{true} ; for inference of χ the posterior using only CH has variance larger than that of the posterior using the joint likelihood, compared to using RT only or the joint likelihood. In psychology and economics, researchers usually focus on the choice data CH in parameters inference of SSMs like MLBA. The figure shows that using response time data in inference not only reduces the approximate posterior variance to make it closer to the true posterior variance, but also helps locate the area of the global maximum. Such conclusions are likely to extend to other variants of MLBA and LBA. Section C.3 of the Supplement details additional experiments on the factors affecting the performance of MOBOLFI in this example.

4.2.3. Real-world data. MOBOLFI is applied to infer parameters of MLBA on a real-world dataset from a consumer choice experiment. This experiment assesses the rental preferences of ride-hailing drivers in Singapore for electric vehicles (EVs) via a street-intercept survey (Ding et al., 2024). Before the stated preference experiment, the driver’s basic information such as working days per week and information about currently rented internal combustion engine vehicles (ICEVs) is collected. The drivers were asked to make a choice among three alternatives including ICEVs, Electric Vehicle Model A (EVA), and Electric Vehicle Model B (EVB) with three listed attributes, which are monthly rental cost (RC, in SGD), daily operating cost (OC, in SGD), and daily mileage (DR, in km). The time that elapses from the appearance of information to the confirmation of choice is recorded as RT. Note that EVA and EVB are assumed to be identical except for their values of three listed attributes. After data preprocessing, 149 participants with 584 valid observations are used in the parameter estimation. Since monthly rental cost (RC) and daily operating cost (OC) capture the monetary aspect, these two can be merged into one alternative specific attribute for the monthly total cost (TC, in SGD).

$$(4.6) \quad TC_{na} = RC_{na} + OC_{na} \times WF_n \times \frac{52}{12},$$

where n and a are the indices of observation and alternative respectively. WF_n is the number of working days per week, hence TC_{na} is the monthly total cost for alternative a in observation n . Lastly, due to the heavy-tailed distribution of DR, it is transformed to log scale. In summary, the size of the attribute matrix X is 584×6 , and the real output data for the MLBA simulator (RT, CH) is 584×4 .

The unknown parameter is $\theta = (\lambda_1, \log \beta_{TC}, \log \beta_{\log DR}, \zeta_{ICEV}, \log(\chi - \mathcal{A}))$, and the rest of the parameters are fixed at known values. Firstly, we set $\mathcal{A} = 45$, $s = 1$, $\zeta_{EVB} = 0$, and $I_0 = 1$ to ensure parameter identification. Secondly, the alternative-specific constant ζ is often interpreted as the initial preference of the corresponding alternative before considering the attribute values in empirical studies. A mild and reasonable assumption made here is that $\zeta_{EVA} = \zeta_{EVB} = 0$, since both are EVs. Furthermore, according to the posterior of λ_2 using the closed-form likelihood when estimable, it is very close to 0, hence, $\lambda_2 = 0$ is used for the final empirical analysis. Section C.4.1 in the Supplement gives detailed results obtained using the closed-form likelihood. Finally, similarly to synthetic data estimation, $\beta_{TC}, \beta_{\log DR}$, and $\chi - \mathcal{A}$ are log-transformed to increase sampling efficiency.

Analogous to the synthetic data, for the implementation of MOBOLFI, 100 initial prior samples $\{\theta^{(i)}, (RT^{(i)}, CH^{(i)})\}_{i=1}^{100}$ are drawn, where $\lambda_1^{(i)} \sim \mathcal{U}[0, 5]$, $\zeta_{ICEV}^{(i)} \sim \mathcal{U}[-3, 5]$, $\log \beta_{TC}^{(i)} \sim \mathcal{U}[-3, 5]$, $\log \beta_{\log DR}^{(i)} \sim \mathcal{U}[-3, 5]$, and $\log(\chi - \mathcal{A})^{(i)} \sim \mathcal{U}[-2, 6]$. The training data is $\{\theta^{(i)}, (\Delta_1^*(RT^{(i)}, RT^o), \Delta_2^*(CH^{(i)}, CH^o))\}_{i=1}^{100}$, where (RT^o, CH^o) are observed

empirical data. Unlike the synthetic data experiment using single simulated RT and CH data for discrepancies by eq. (4.4) and eq. (4.5), $(RT^{(i)}, CH^{(i)}) = \{(RT_s^{(i)}, CH_s^{(i)})\}_{s=1}^S$ is a collection of multiple simulations independently generated by the MLBA simulator with $\theta^{(i)}$ and attribute matrix X . The discrepancy for the RT data source $\Delta_1^*(RT^{(i)}, RT^o)$ is the average of 1-Wasserstein distance between the empirical distribution of log-transformed RT^o and the replicates of $RT^{(i)}$:

$$(4.7) \quad \Delta_1^*(RT^{(i)}, RT^o) = \frac{\sum_{s=1}^S \|\log(\widetilde{RT}^o) - \log(\widetilde{RT}_s^{(i)})\|_1}{S}.$$

The discrepancy $\Delta_2^*(CH^{(i)}, CH^o)$ for the choice data is the Brier score (Brier, 1950) between the empirical probabilities over the $S = 30$ replicates for the synthetic choice data and the observed choice outcomes (i.e. the average squared difference between empirical probabilities by simulations and observed outcomes):

$$(4.8) \quad \Delta_2^*(CH^{(i)}, CH^o) = \frac{1}{3 \times 584} \sum_{j=1}^{584} \left(CH_j^o - \frac{\sum_{s=1}^S CH_{sj}^{(i)}}{S} \right)^2.$$

There are two reasons for adopting Δ^* instead of Δ in eq.(4.4) and eq.(4.5) for the empirical experiment. Firstly, for the CH discrepancy, the Brier score in eq.(4.8) offers a more informative discrepancy by capturing the empirical choice distribution $\frac{\sum_{s=1}^S CH_s^{(i)}}{S}$ rather than a chosen instance. Secondly, for both RT and CH discrepancies, Δ_1^* and Δ_2^* offer more robust discrepancies than Δ thanks to averaging over S replicates. Consequently, Δ_1^* and Δ_2^* result in a quicker convergence during MOBOLFI GP model training while requiring S times as many model simulations per acquisition as Δ_1 and Δ_2 . For a comparison between Δ and Δ^* , see Section C.4.2 of the Supplement. De-MCMC is used for both the MOBOLFI approximate posterior and closed-form MLBA posterior estimation.

Figure 5 shows approximate marginal MOBOLFI posteriors for selected parameters and the corresponding posteriors for the closed-form MLBA likelihood. The figure demonstrates that the contributions of different data sources to the estimation of individual parameters can vary greatly according to the parameter, and MOBOLFI can reveal these relationships. For example, the MOBOLFI marginal posterior of δ_{ICEV} is very diffuse when conditioning on only response-time data, showing that the MOBOLFI posterior conditioning on both data sources is informative mostly because of the choice data. This aligns with the interpretation from psychology that δ stands for the initially rooted preference for an alternative before taking a survey which is independent of the decision-making process, hence rarely captured by RT data only. On the other hand, the $\log(\chi - \mathcal{A})$ MOBOLFI marginal posterior conditioning on both choice and response time is more similar to its marginal posterior conditional on response time only. This is consistent with the interpretation that χ reflects the decision difficulty and respondent's cautiousness, which are associated with RT. In addition, the marginal MOBOLFI posteriors of $\log \beta_{TC}$, $\log \beta_{\log DR}$, and λ_1 display large variance and different patterns from the closed-form posterior. Section C.4.3 in the Supplement shows a similar distribution of the discrepancies using the closed-form and joint MOBOLFI MAP estimates, and also demonstrate that the distribution of the discrepancy depends weakly on $\log \beta_{TC}$, $\log \beta_{\log DR}$ and λ_1 .

5. Discussion. We developed Multi-objective Bayesian Optimization for Likelihood-Free Inference (MOBOLFI) to address Bayesian inference with multi-source data in complex models with intractable likelihood, such as SSMs. MOBOLFI extends the classic BOLFI method, which acquires model simulations at the most beneficial parameter values by using Bayesian optimization (BO) applied to minimization of an expected discrepancy between

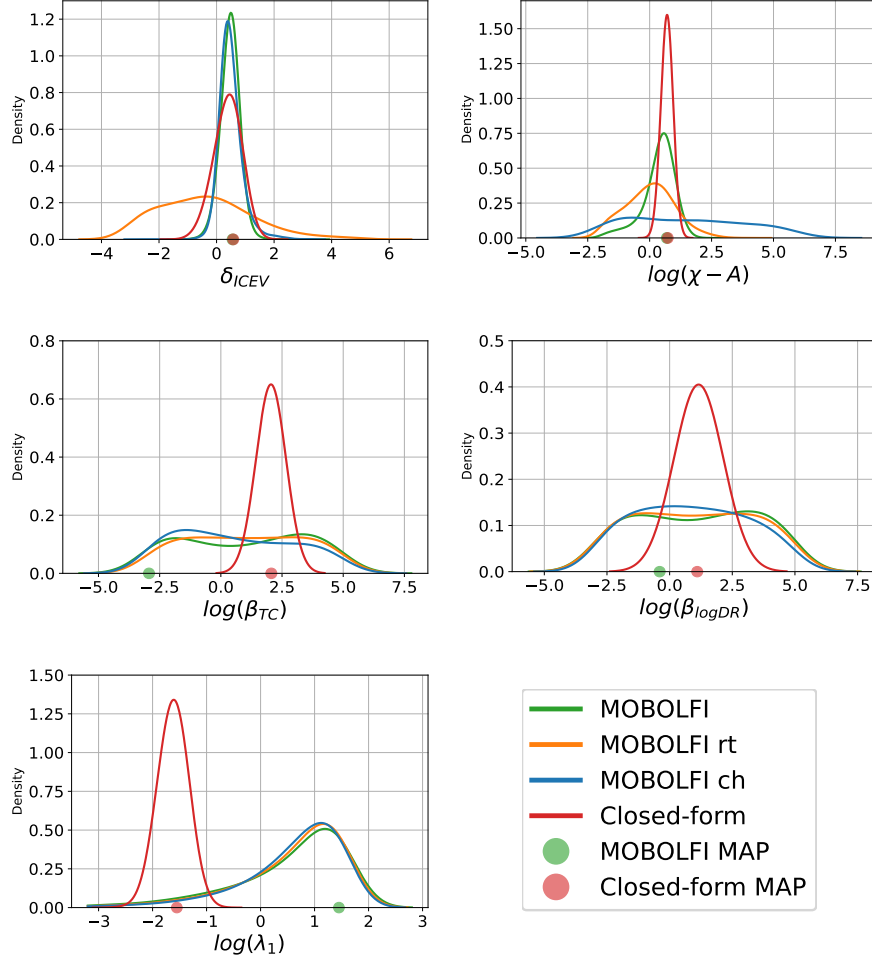


Figure 5: Approximate and closed-form posteriors with MAPs of MLBA example. Each plot from the figure shows the marginal posterior of the parameter of interest. The green curve represents the MOBOLFI approximate posterior for joint data sources. The orange/blue curve shows the marginal MOBOLFI approximate posterior for RT /CH data, respectively. The green dot is the maximum a posteriori probability (MAP) estimate sought over all MCMC samplers of the joint MOBOLFI approximate posterior. The red curve shows the closed-form posterior conditional on both data sources, i.e. product closed-for likelihood of both data sources and a Uniform prior. The red dot denotes the MAP estimated by closed-form MLBA posterior with the same sampling strategy. The parameter λ_1 has been transformed to log scale to more easily compare the marginal posteriors for this parameter for different methods.

synthetic and observed data. The surrogate model used in BOLFI is also used for approximating the likelihood. The MOBOLFI extension for multi-source data considers a discrepancy for each data source, and considers multi-objective BO for exploring the parameter values where any individual data source likelihood is high in a simulation efficient manner. Major advantages of the approach include avoiding information loss from naive methods for combination of data-source specific discrepancies into a single discrepancy, and the ability to approximate both the joint likelihood and likelihood for individual data sources. The latter is

useful for detecting conflict between data sources, and for understanding the importance of the data sources for estimation of individual parameters.

Although the MOBOLFI method is motivated by the parameter inference of SSMs with multi-source data, it can be applied to Likelihood-Free inference of other complex models. For example, in Section D of the Supplement we consider an example on bacterial infection in day care centres where parameters of a latent Markov process are inferred. We partition 4 data summaries into two and apply MOBOLFI for inference. MOBOLFI is competitive with BOLFI even in this example with only an individual data source. For the case of SSMs, we use the MLBA simulator as the simulator of interest in our experiments, and MOBOLFI could be used in a wide range of SSM variants, especially for those whose likelihood functions are intractable like DDM, MDFT, etc. An interesting direction for future work is to consider different choices of the acquisition function in the MOBOLFI approach. Multi-objective BO is an active area of research in Bayesian optimization, and new developments in BO methodology may translate into improved performance in Likelihood-Free applications. State-of-art computational methods for the MLBA with closed-form likelihood, including variants of the model including random effects, are discussed in [Gunawan et al. \(2020\)](#), and [Evans \(2019\)](#) addresses the important issue of efficient simulation from various SSM models, which is particularly important for Likelihood-Free inference.

In applying MOBOLFI there are a number of challenges. One is that the initialization of the algorithm can be very important, and an adequate initial covering of the space is needed. This seems to be especially crucial with acquisition functions based on expected hypervolume improvement, where the BO algorithm can keep proposing points in a small area of the space without a proper initialization. Another difficulty, common to many other LFI algorithms, is the choice of data summary statistics used to define discrepancies. In Section C.4 of the Supplement we consider alternative choices of summary statistics to the ones considered in section 4.2.2 based on auxiliary model approaches to summary statistic construction which are widely used in the ABC literature (e.g. [Drovandi, Pettitt and Lee 2015](#)). Further exploration of these challenges is left to future work.

6. Acknowledgement. David Nott’s research was supported by the Ministry of Education, Singapore, under the Academic Research Fund Tier 2 (MOE-T2EP20123-0009), and he is affiliated with the Institute of Operations Research and Analytics at the National University of Singapore.

REFERENCES

- AN, Z., NOTT, D. J. and DROVANDI, C. (2020). Robust Bayesian synthetic likelihood via a semi-parametric approach. *Statistics and Computing* **30** 543–557.
- AUSHEV, A., PESONEN, H., HEINONEN, M., CORANDER, J. and KASKI, S. (2022). Likelihood-free inference with deep Gaussian processes. *Computational Statistics and Data Analysis* **174** 107529. <https://doi.org/10.1016/j.csda.2022.107529>
- BALANDAT, M., KARRER, B., JIANG, D., DAULTON, S., LETHAM, B., WILSON, A. G. and BAKSHY, E. (2020). BoTorch: A Framework for Efficient Monte-Carlo Bayesian Optimization. In *Advances in Neural Information Processing Systems* (H. LAROCHELLE, M. RANZATO, R. HADSELL, M. F. BALCAN and H. LIN, eds.) **33** 21524–21538. Curran Associates, Inc.
- BANSAL, P., KIM, E.-J. and OZDEMIR, S. (2024). Discrete choice experiments with eye-tracking: How far we have come and ways forward. *Journal of Choice Modelling* **51** 100478.
- BLIZNYUK, N., RUPPERT, D., SHOEMAKER, C., REGIS, R., WILD, S. and MUGUNTHAN, P. (2008). Bayesian Calibration and Uncertainty Analysis for Computationally Expensive Models Using Optimization and Radial Basis Function Approximation. *Journal of Computational and Graphical Statistics* **17** 270-294. <https://doi.org/10.1198/106186008X320681>
- BRIER, G. W. (1950). Verification of forecasts expressed in terms of probability. *Monthly Weather Review* **78** 1-3.

- BROWN, S. D. and HEATHCOTE, A. (2008). The simplest complete model of choice response time: Linear ballistic accumulation. *Cognitive psychology* **57** 153–178.
- CAPLIN, A. (2016). Measuring and modeling attention. *Annual Review of Economics* **8** 379–403.
- CHEREMUKHIN, A., POPOVA, A. and TUTINO, A. (2015). A theory of discrete choice with information costs. *Journal of Economic Behavior & Organization* **113** 34–50.
- CLITHERO, J. A. (2018). Improving out-of-sample predictions using response times and a model of the decision process. *Journal of Economic Behavior & Organization* **148** 344–375.
- COBB, A. D. and JALAIAN, B. (2021). Scaling Hamiltonian Monte Carlo Inference for Bayesian Neural Networks with Symmetric Splitting. *Uncertainty in Artificial Intelligence*.
- CONRAD, P. R., MARZOUK, Y. M., PILLAI, N. S. and SMITH, A. (2016). Accelerating Asymptotically Exact MCMC for Computationally Intensive Models via Local Approximations. *Journal of the American Statistical Association* **111** 1591–1607. <https://doi.org/10.1080/01621459.2015.1096787>
- COX, D. D. and JOHN, S. (1997). SDO: A statistical method for global optimization. In *Multidisciplinary Design Optimization: State of the Art* 315–329. SIAM: Philadelphia.
- CRAIG, P. S., GOLDSTEIN, M., SEHEULT, A. H. and SMITH, J. A. (1997). Pressure matching for hydrocarbon reservoirs: a case study in the use of Bayes linear strategies for large computer experiments. In *Case Studies in Bayesian Statistics: Volume III* 37–93. Springer.
- DAULTON, S., BALANDAT, M. and BAKSHY, E. (2021a). Parallel Bayesian Optimization of Multiple Noisy Objectives with Expected Hypervolume Improvement. In *Advances in Neural Information Processing Systems* (M. RANZATO, A. BEYGELZIMER, Y. DAUPHIN, P. S. LIANG and J. W. VAUGHAN, eds.) **34** 2187–2200. Curran Associates, Inc.
- DAULTON, S., BALANDAT, M. and BAKSHY, E. (2021b). Parallel Bayesian optimization of multiple noisy objectives with expected hypervolume improvement. *Advances in Neural Information Processing Systems* **34** 2187–2200.
- DING, J., KIM, E.-J., MAKSIMENKO, V. and BANSAL, P. (2024). Can Decoy Effects Nudge Ride-hailing Drivers' Preferences for Electric Vehicles? Available at SSRN 4682413.
- DROVANDI, C. C., PETTITT, A. N. and LEE, A. (2015). Bayesian Indirect Inference Using a Parametric Auxiliary Model. *Statistical Science* **30** 72 – 95.
- EMMERICH, M. (2005). Single-and multi-objective evolutionary design optimization assisted by gaussian random field metamodels, PhD thesis, Fachbereich Informatik, University of Dortmund.
- EVANS, N. J. (2019). A method, framework, and tutorial for efficiently simulating models of decision-making. *Behavior Research Methods* **51** 2390–2404.
- EVANS, M. and MOSHONOV, H. (2006). Checking for prior-data conflict. *Bayesian Analysis* **1** 893–914.
- FASIOLO, M., WOOD, S. N., HARTIG, F. and BRAVINGTON, M. V. (2018). An extended empirical saddlepoint approximation for intractable likelihoods. *Electronic Journal of Statistics* **12** 1544 – 1578.
- FIELDING, M., NOTT, D. J. and LIONG, S.-Y. (2011). Efficient MCMC Schemes for Computationally Expensive Posterior Distributions. *Technometrics* **53** 16–28. <https://doi.org/10.1198/TECH.2010.09195>
- FRAZIER, D. T., NOTT, D. J., DROVANDI, C. and KOHN, R. (2022). Bayesian inference using synthetic likelihood: asymptotics and adjustments. *Journal of the American Statistical Association* **118** 2821–2832.
- GARNETT, R. (2023). *Bayesian Optimization*. Cambridge University Press. <https://doi.org/10.1017/9781108348973>
- GILBRIDE, T. J. and ALLENBY, G. M. (2004). A choice model with conjunctive, disjunctive, and compensatory screening rules. *Marketing Science* **23** 391–406.
- GREENBERG, D. S., NONNENMACHER, M. and MACKE, J. H. (2019). Automatic Posterior Transformation for Likelihood-Free Inference. In *Proceedings of the 36th International Conference on Machine Learning, ICML 2019, 9-15 June 2019, Long Beach, California, USA* (K. CHAUDHURI and R. SALAKHUTDINOV, eds.). *Proceedings of Machine Learning Research* **97** 2404–2414. PMLR.
- GUNAWAN, D., HAWKINS, G. E., TRAN, M. N., KOHN, R. and BROWN, S. D. (2020). New estimation approaches for the hierarchical Linear Ballistic Accumulator model. *Journal of Mathematical Psychology* **96** 102368.
- GUTMANN, M. U. and CORANDER, J. (2016). Bayesian Optimization for Likelihood-Free Inference of Simulator-Based Statistical Models. *Journal of Machine Learning Research* **17** 1–47.
- HANCOCK, T. O., HESS, S. and CHOUDHURY, C. F. (2018). Decision field theory: Improvements to current methodology and comparisons with standard choice modelling techniques. *Transportation Research Part B: Methodological* **107** 18–40.
- HANCOCK, T. O., HESS, S., MARLEY, A. A. and CHOUDHURY, C. F. (2021a). An accumulation of preference: two alternative dynamic models for understanding transport choices. *Transportation Research Part B: Methodological* **149** 250–282.

- HANCOCK, T. O., HESS, S., MARLEY, A. A. J. and CHOUDHURY, C. F. (2021b). An accumulation of preference: Two alternative dynamic models for understanding transport choices. *Transportation Research Part B: Methodological* **149** 250–282. <https://doi.org/10.1016/j.trb.2021.04.001>
- HEITZ, R. P. (2014). The speed-accuracy tradeoff: history, physiology, methodology, and behavior. *Frontiers in neuroscience* **8** 86875.
- JÄRVENPÄÄ, M. and CORANDER, J. (2021). Approximate Bayesian inference from noisy likelihoods with Gaussian process emulated MCMC.
- JÄRVENPÄÄ, M., GUTMANN, M. U., VEHTARI, A. and MARTTINEN, P. (2018). Gaussian process modelling in approximate Bayesian computation to estimate horizontal gene transfer in bacteria. *The Annals of Applied Statistics* **12** 2228 – 2251. <https://doi.org/10.1214/18-AOAS1150>
- JÄRVENPÄÄ, M., GUTMANN, M. U., PLESKA, A., VEHTARI, A. and MARTTINEN, P. (2019). Efficient Acquisition Rules for Model-Based Approximate Bayesian Computation. *Bayesian Analysis* **14** 595 – 622. <https://doi.org/10.1214/18-BA1121>
- JÄRVENPÄÄ, M., GUTMANN, M. U., VEHTARI, A. and MARTTINEN, P. (2021). Parallel Gaussian Process Surrogate Bayesian Inference with Noisy Likelihood Evaluations. *Bayesian Analysis* **16** 147 – 178. <https://doi.org/10.1214/20-BA1200>
- KANDASAMY, K., SCHNEIDER, J. and POZOS, B. (2015). Bayesian Active Learning for Posterior Estimation In *Proceedings of 24th International Joint Conference on Artificial Intelligence (IJCAI '15)* 3605 - 3611.
- KENNEDY, M. C. and O'HAGAN, A. (2001). Bayesian calibration of computer models. *Journal of the Royal Statistical Society: Series B (Statistical Methodology)* **63** 425-464. <https://doi.org/10.1111/1467-9868.00294>
- LEWIS, J. R., MACEACHERN, S. N. and LEE, Y. (2021). Bayesian Restricted Likelihood Methods: Conditioning on Insufficient Statistics in Bayesian Regression (with Discussion). *Bayesian Analysis* **16** 1393 – 2854.
- MARSHALL, E. C. and SPIEGELHALTER, D. J. (2007). Identifying outliers in Bayesian hierarchical models: a simulation-based approach. *Bayesian Analysis* **2** 409–444.
- MEEDS, E. and WELLING, M. (2014). GPS-ABC: Gaussian Process Surrogate Approximate Bayesian Computation. In *Proceedings of the Thirtieth Conference on Uncertainty in Artificial Intelligence, UAI 2014, Quebec City, Quebec, Canada, July 23-27, 2014* (N. L. ZHANG and J. TIAN, eds.) 593–602. AUAI Press.
- NOGUCHI, T. and STEWART, N. (2018). Multialternative decision by sampling: A model of decision making constrained by process data. *Psychological review* **125** 512.
- NUMMINEN, E., CHENG, L., GYLLENBERG, M. and CORANDER, J. (2013). Estimating the transmission dynamics of Streptococcus pneumoniae from strain prevalence data. *Biometrics* **69** 748–757.
- PAPAMAKARIOS, G. and MURRAY, I. (2016). Fast ϵ -free Inference of Simulation Models with Bayesian Conditional Density Estimation. In *Advances in Neural Information Processing Systems* (D. LEE, M. SUGIYAMA, U. LUXBURG, I. GUYON and R. GARNETT, eds.) **29**. Curran Associates, Inc.
- PAPAMAKARIOS, G., STERRATT, D. and MURRAY, I. (2019). Sequential Neural Likelihood: fast Likelihood-free Inference with Autoregressive Flows. In *Proceedings of the Twenty-Second International Conference on Artificial Intelligence and Statistics* (K. CHAUDHURI and M. SUGIYAMA, eds.). *Proceedings of Machine Learning Research* **89** 837–848. PMLR.
- PISAURO, M. A., FOURAGNAN, E., RETZLER, C. and PHILIASTIDES, M. G. (2017). Neural correlates of evidence accumulation during value-based decisions revealed via simultaneous EEG-fMRI. *Nature communications* **8** 15808.
- PRESANIS, A. M., OHLSSSEN, D., SPIEGELHALTER, D. J. and ANGELIS, D. D. (2013). Conflict Diagnostics in Directed Acyclic Graphs, with Applications in Bayesian Evidence Synthesis. *Statistical Science* **28** 376–397.
- PRICE, L. F., DROVANDI, C. C., LEE, A. C. and NOTT, D. J. (2018). Bayesian synthetic likelihood. *Journal of Computational and Graphical Statistics* **27** 1-11.
- RADEV, S. T., SCHMITT, M., SCHUMACHER, L., ELSEMÜLLER, L., PRATZ, V., SCHÄLTE, Y., KÖTHE, U. and BÜRKNER, P.-C. (2023). BayesFlow: Amortized Bayesian Workflows With Neural Networks. *Journal of Open Source Software* **8** 5702. <https://doi.org/10.21105/joss.05702>
- RASMUSSEN, C. (2003). Gaussian Processes to Speed up Hybrid Monte Carlo for Expensive Bayesian Integrals. 651-659. Max-Planck-Gesellschaft.
- RATCLIFF, R., SMITH, P. L., BROWN, S. D. and MCKOON, G. (2016). Diffusion decision model: Current issues and history. *Trends in cognitive sciences* **20** 260–281.
- SCHMITT, M., RADEV, S. T. and BÜRKNER, P.-C. (2023). Fuse It or Lose It: Deep Fusion for Multimodal Simulation-Based Inference. *arXiv preprint arXiv:2311.10671*.
- SHIMOJO, S., SIMION, C., SHIMOJO, E. and SCHEIER, C. (2003). Gaze bias both reflects and influences preference. *Nature neuroscience* **6** 1317–1322.
- SISSON, S. A., FAN, Y. and BEAUMONT, M. A., eds. (2018). *Handbook of Approximate Bayesian Computation*. Chapman & Hall/CRC.
- SMITH, P. L. (2000). Stochastic dynamic models of response time and accuracy: A foundational primer. *Journal of mathematical psychology* **44** 408–463.

- SRINIVAS, N., KRAUSE, A., KAKADE, S. M. and SEEGER, M. (2009). Gaussian process optimization in the bandit setting: No regret and experimental design. *arXiv preprint arXiv:0912.3995*.
- SRINIVAS, N., KRAUSE, A., KAKADE, S. M. and SEEGER, M. W. (2012). Information-theoretic regret bounds for gaussian process optimization in the bandit setting. *IEEE transactions on information theory* **58** 3250–3265.
- TERRY, A., MARLEY, A. A. J., BARNWAL, A., WAGENMAKERS, E. J., HEATHCOTE, A. and BROWN, S. D. (2015). Generalising the drift rate distribution for linear ballistic accumulators. *Journal of Mathematical Psychology* **68-69** 49–58. <https://doi.org/10.1016/j.jmp.2015.09.002>
- THOMAS, O., SÁ-LEÃO, R., DE LENCASTRE, H., KASKI, S., CORANDER, J. and PESONEN, H. (2020). Misspecification-robust likelihood-free inference in high dimensions.
- TRUEBLOOD, J. S., BROWN, S. D. and HEATHCOTE, A. (2014). The multiattribute linear ballistic accumulator model of context effects in multialternative choice. *Psychological review* **121** 179.
- TURNER, B. M. and SEDERBERG, P. B. (2014). A generalized, likelihood-free method for posterior estimation. *Psychonomic bulletin & review* **21** 227–250.
- TURNER, B. M., SEDERBERG, P. B., BROWN, S. D. and STEYVERS, M. (2013). A method for efficiently sampling from distributions with correlated dimensions. *Psychological methods* **18** 368.
- WILKINSON, R. (2014). Accelerating ABC methods using Gaussian processes. In *Proceedings of the Seventeenth International Conference on Artificial Intelligence and Statistics* (S. KASKI and J. CORANDER, eds.). *Proceedings of Machine Learning Research* **33** 1015–1023. PMLR, Reykjavik, Iceland.
- WOOD, S. N. (2010). Statistical inference for noisy nonlinear ecological dynamic systems. *Nature* **466** 1102–1104.

Supplement

A. Derivation of Methods & details of implementation.

A.1. *Gaussian Processes and Bayesian optimization.* Here we provide further background on Gaussian processes and Bayesian optimization (BO). To make the discussion self-contained, there is some repetition of definitions and concepts explained in the main text. BO with a Gaussian process surrogate is used in the BOLFI method which inspires the new MOBOLFI approach in our work.

Bayesian optimization attempts to find a global optimum of a function. We will consider Bayesian optimization for finding a global minimum. We want to minimize $f(\theta)$, $\theta \in \Theta \subseteq \mathbb{R}^p$, where derivatives of $f(\cdot)$ are not available, and evaluations of $f(\cdot)$ may be corrupted by noise. BO is most suitable for problems where the dimension of θ is not too large, although high-dimensional BO is an active area of current research. We model the noisy evaluations of $f(\theta)$ with a ‘‘surrogate model’’ describing uncertainty about $f(\cdot)$ given the function evaluations previously made. A common surrogate model in BO is a Gaussian process, and this is used in the BOLFI method.

We establish some notation and definitions first. Suppose that $\tilde{\Theta}$ is an $n \times p$ matrix, with i th row $\tilde{\theta}_i \in \Theta$. For any function $g : \Theta \rightarrow \mathbb{R}$, we write $g(\tilde{\Theta})$ for the vector obtained by applying $g(\cdot)$ to the rows of $\tilde{\Theta}$, i.e. $g(\tilde{\Theta}) = (g(\tilde{\theta}_1), \dots, g(\tilde{\theta}_n))^\top$. Suppose that $\bar{\Theta}$ is an $m \times p$ matrix, where the i th row is $\bar{\theta}_i \in \Theta$. For any function $h : \Theta \times \Theta \rightarrow \mathbb{R}$, we write $h(\tilde{\Theta}, \bar{\Theta})$ for the $n \times m$ matrix with (i, j) th entry $h(\tilde{\theta}_i, \bar{\theta}_j)$. For $\theta_1, \dots, \theta_n \in \Theta$, denote by $\theta_{1:n}$ the $n \times p$ matrix with i th row θ_i . A random function $f(\cdot)$ defined on Θ is a Gaussian process with mean function $\mu : \Theta \rightarrow \mathbb{R}$ and positive definite covariance function $C : \Theta \times \Theta \rightarrow \mathbb{R}$ if, for any n , and any $\theta_1, \dots, \theta_n \in \Theta$, the random vector $f(\theta_{1:n})$ is multivariate normally distributed, $f(\theta_{1:n}) \sim N(\mu(\theta_{1:n}), C(\theta_{1:n}, \theta_{1:n}))$.

Suppose we observe the Gaussian process $f(\cdot)$ with noise at points $\theta_1, \dots, \theta_n \in \Theta$. The noisy observations are

$$(A.1) \quad z_i = f(\theta_i) + \epsilon_i, \quad i = 1, \dots, n,$$

where $\epsilon_i \stackrel{iid}{\sim} N(0, \sigma^2)$, for some variance $\sigma^2 > 0$. In many applications, the Gaussian noise assumption can be reasonable in the vicinity of the minimizer with an appropriate transformation. Write $z_{\leq n} = (z_1, \dots, z_n)^\top$. We are interested in describing uncertainty about $f(\theta^*)$ for some $\theta^* \in \Theta$, given the noisy observations $z_{\leq n}$. Since $f(\cdot)$ is a Gaussian process with mean function $\mu(\cdot)$ and covariance function $C(\cdot, \cdot)$, $(f(\theta_{1:n})^\top, f(\theta^*))^\top$ is multivariate normal, and because of the independent normally distributed noise in (A.1), $(z_{\leq n}^\top, f(\theta^*))^\top$ is easily shown to be multivariate normal. It follows that $f(\theta^*)|z_{\leq n} \sim N(\mu_n(\theta^*), \sigma_n^2(\theta^*))$, where

$$(A.2) \quad \mu_n(\theta^*) = \mu(\theta^*) + C(\theta^*, \theta_{1:n}) \{C(\theta_{1:n}, \theta_{1:n}) + \sigma^2 I\}^{-1} (z_{\leq n} - \mu(\theta_{1:n})),$$

$$(A.3) \quad \sigma_n^2(\theta^*) = C(\theta^*, \theta^*) - C(\theta^*, \theta_{1:n}) \{C(\theta_{1:n}, \theta_{1:n}) + \sigma^2 I\}^{-1} C(\theta_{1:n}, \theta^*).$$

The uncertainty quantification provided by (A.2) and (A.3) can be used to decide which θ^* should be used to obtain a further noisy observation

$$z^* = f(\theta^*) + \epsilon^*, \quad \epsilon^* \sim N(0, \sigma^2),$$

having the most benefit in the search for the minimizer. θ^* is chosen through an optimization, of the ‘‘acquisition function’’. This acquisition function can be the expected loss for some formal decision problem where the expectation is taken with respect to the the Gaussian process uncertainty about $f(\cdot)$, or it might be chosen using more heuristic reasoning.

In the BOLFI method, [Gutmann and Corander \(2016\)](#) suggested using the lower confidence bound acquisition function ([Cox and John, 1997](#)),

$$(A.4) \quad A_n(\theta) = \mu_n(\theta) - \sqrt{\eta_n^2 \sigma_n^2(\theta)},$$

where

$$\eta_n^2 = 2 \log \left(n^{\frac{p}{2}+2} \frac{\pi^2}{3\epsilon_\eta} \right),$$

with the default value $\epsilon_\eta = 0.1$. With such design of the η_n^2 , the cumulative regret of a GP using Upper Confidence bound as the acquisition is proved to be bounded with high probability ([Srinivas et al., 2009](#)). In the day care center example discussed in Section 4, we implement BOLFI using η_n^2 . However, in the two examples presented in the main text, the large number of parameters p results in a large η_n^2 . This increases the probability that the acquisition point is not close to the global optimum, necessitating more iterations and longer training times for the implementation of BOLFI. Additionally, this approach risks proposing points outside the range of the uniform prior, potentially leading to numerical problems. To ensure numerical stability and efficient training, for the two examples in main text, we replace η_n^2 with

$$\eta_n^{2*} = 2 \log \left(n^2 \frac{\pi^2}{3\epsilon_\eta} \right).$$

We posit that using η_n^{2*} specifically for these examples strikes an effective balance between exploration and exploitation.

Further discussion of the intuitive basis for this acquisition function is given in the main text. We have described the process of choosing a new location for taking a new noisy function evaluation in BO algorithms. To completely specify a BO algorithm, we need to describe a method of initialization (where some initial function values are obtained, perhaps using a space-filling design on Θ), a stopping rule (most simply we might stop when a given budget of function evaluations is exhausted) and a method for estimating Gaussian process hyperparameters, and updating estimates as the algorithm proceeds. For further details on these practical issues see, for example [Garnett \(2023\)](#). For the two examples in the main text, we considered different initializations, with details given in Sections 2.1 and 3.2.

A.2. Related work on BOLFI. The BOLFI approach of [Gutmann and Corander \(2016\)](#) has been very successful for simulation efficient estimation of posterior distributions with expensive simulators, and the basic method has been further developed in a number of ways. [Järvenpää et al. \(2018\)](#), explores the importance of the Gaussian process formulation used in the BOLFI framework, including transformations of the discrepancy, heteroskedastic or classifier Gaussian process formulations for likelihood approximations, and different utilities for Gaussian process model choice. [Järvenpää et al. \(2019\)](#) go beyond generic acquisition functions from the Bayesian optimization literature and develop alternatives tailored to simulation-based inference problems targeting the reduction of posterior uncertainty. [Järvenpää et al. \(2021\)](#) consider Bayesian optimization for likelihood-free inference with noisy log-likelihood evaluations and batch sequential strategies amenable to parallel computation. [Aushev et al. \(2022\)](#) consider replacing the Gaussian process used in BOLFI with a deep Gaussian process, and demonstrate that this can result in more accurate posterior approximations, particularly when the target posterior density is multi-modal. [Kandasamy, Schneider and Póczos \(2015\)](#) use Bayesian optimization with some novel acquisition functions to query an expensive to evaluate likelihood, before estimating the posterior using the cheap to evaluate surrogate. A generalized Bayesian version of BOLFI, which is suitable for mis-specified

models and when the summary statistic dimension is high, is described by [Thomas et al. \(2020\)](#).

The use of a Gaussian process or other ‘‘surrogate’’ models to obtain a likelihood approximation is not only used in the context of BO methods. [Wilkinson \(2014\)](#) considers a Gaussian process surrogate for a synthetic likelihood ([Wood, 2010](#); [Price et al., 2018](#)) in so-called history matching algorithms ([Craig et al., 1997](#)). [Meeds and Welling \(2014\)](#) consider Gaussian process surrogate models for summary statistic means and variances for a synthetic likelihood, and adaptively acquire simulations in order to reduce uncertainty in a Metropolis-Hastings accept/reject decision for posterior simulation. A similar more sophisticated approach has recently been considered by [Järvenpää and Corander \(2021\)](#), where the authors use a Gaussian process surrogate for the log-likelihood itself, and are more explicit about acquisition rules for augmenting the training set for the Gaussian process. A surrogate model can be useful too in applications where exact likelihood calculations can be made, but are expensive. See, for example, [Kennedy and O’Hagan \(2001\)](#); [Rasmussen \(2003\)](#); [Bliznyuk et al. \(2008\)](#); [Fielding, Nott and Liang \(2011\)](#); [Conrad et al. \(2016\)](#) among many others.

A.3. Implementation of MOBOLFI. Here we give details of multi-objective Bayesian optimization which are not given in the main text. Multi-objective BO is used in implementing the MOBOLFI method developed in the main text. Once again, there is some repetition with definitions and concepts in the main text to make the discussion self-contained.

Let $f(\theta) = (f_1(\theta), \dots, f_K(\theta))^\top$ be a multivariate function, for which we are interested in minimizing the components of $f(\cdot)$. In general there is no value $\theta^* \in \Theta$ where all components are minimized simultaneously. Multi-objective optimization methods approximate the set of ‘‘non-dominated’’ solutions which are not obviously inferior to other solutions. A value $\theta \in \Theta$ dominates $\theta' \in \Theta$ if $f_j(\theta) \leq f_j(\theta')$, $j = 1, \dots, K$, with the inequality being strict for at least one j . The dominated solution is inferior in the sense that there is another point at which $f(\cdot)$ is strictly smaller along some dimensions and no larger for the other dimensions. Multi-objective optimization algorithms try to find the Pareto optimal set of non-dominated points in Θ .

Numerical multi-objective optimization methods obtain finite approximations to the Pareto set. The Pareto frontier is the set of optimal function values obtained by the points in the Pareto set. Multi-objective Bayesian optimization ([Garnett, 2023](#), Section 11.7) uses surrogate models to implement multi-objective optimization for expensive to evaluate functions, possibly observed with noise. Similar to Bayesian optimization with a scalar objective, the representation of uncertainty given by the surrogate is used to efficiently decide where to perform the next function evaluation.

Multivariate Gaussian processes are a common choice of surrogate for multi-objective Bayesian optimization, and we give some background and notation now, extending the discussion of Section 2.3. Suppose that $g : \Theta \rightarrow \mathbb{R}^K$, and that $\tilde{\Theta}$ is an $n \times p$ matrix with i th row $\tilde{\theta}_i \in \Theta$. We write $g(\tilde{\Theta}) = (g(\tilde{\theta}_1)^\top, \dots, g(\tilde{\theta}_n)^\top)^\top \in \mathbb{R}^{Kn}$. Let $h : \Theta \times \Theta \rightarrow \mathbb{R}^{K \times K}$ be a $K \times K$ matrix-valued function. Let $\bar{\theta}$ be an $n \times m$ matrix with i th row $\bar{\theta}_i$. We write $h(\tilde{\theta}, \bar{\theta})$ for the partitioned matrix with n block rows and m block columns where the (i, j) th block entry is $h(\tilde{\theta}_i, \bar{\theta}_j) \in \mathbb{R}^{K \times K}$. A random function $f(\cdot) = (f_1(\cdot), \dots, f_K(\cdot))^\top$ is a multivariate Gaussian process with mean function $\mu : \Theta \rightarrow \mathbb{R}^K$ and positive definite covariance function $C : \Theta \times \Theta \rightarrow \mathbb{R}^{K \times K}$ if for any n and $\theta_1, \dots, \theta_n$, $f(\theta_{1:n})$ is multivariate normal, $N(\mu(\theta_{1:n}), C(\theta_{1:n}, \theta_{1:n}))$.

Once again extending the discussion of Section 2.2, suppose we observe values of $f(\cdot)$ with noise at $\theta_1, \dots, \theta_n \in \Theta$, to obtain

$$(A.5) \quad z_i = f(\theta_i) + \epsilon_i,$$

where now $z_i \in \mathbb{R}^K$ and $\epsilon_i \stackrel{iid}{\sim} N(0, \Sigma)$ where $\Sigma \in \mathbb{R}^{K \times K}$ is some positive definite covariance matrix. As in our discussion of the univariate case, for some $\theta^* \in \Theta$, and writing $z_{\leq n} = (z_1^\top, \dots, z_n^\top)^\top$, $(z_{\leq n}^\top, f(\theta^*)^\top)^\top$ is multivariate Gaussian and the conditional density of $f(\theta^*)|z_{\leq n}$ is multivariate normal with mean vector and covariance matrix

$$(A.6) \quad \mu_n(\theta^*) = \mu(\theta^*) + C(\theta^*, \theta_{1:n}) \{C(\theta_{1:n}, \theta_{1:n}) + D_n(\Sigma)\}^{-1} (z_{\leq n} - \mu(\theta_{1:n}))$$

$$(A.7) \quad \Sigma_n(\theta^*) = C(\theta^*, \theta^*) - C(\theta^*, \theta_{1:n}) \{C(\theta_{1:n}, \theta_{1:n}) + D_n(\Sigma)\}^{-1} C(\theta_{1:n}, \theta^*),$$

where $D_n(\Sigma) \in \mathbb{R}^{nK \times nK}$ is the block diagonal matrix with the $K \times K$ diagonal block entries equal to Σ . For reducing computation cost, in our later numerical experiments we consider multivariate Gaussian processes where the components of $f(\cdot)$ are independent, but we consider correlated noise in (A.5) i.e. Σ is not diagonal.

The noise ϵ_i can be observed by the variation of repeated simulation $\{z_{i,j}\}_{j=1}^{n_\Sigma}$ give input θ_i . Therefore, the dependent noise covariance matrix Σ is estimated by the covariance of a repeated finite simulation sample $\{\Delta_{i_\Sigma, j}\}_{j=1}^{n_\Sigma}$, where $\Delta_{i_\Sigma, j} = D(\theta_{i_\Sigma}) + \epsilon_{i_\Sigma}$ for some θ_{i_Σ} is a simulated bivariate noisy discrepancy. For results in this paper, we set $n_\Sigma = 100$ and $\theta_{i_\Sigma} = \arg \min_{(\theta_i, \Delta_i) \in T_{n_f}} (\Delta_i - \mu_{n_f}(\theta_i))^\top \Sigma_{n_f}(\theta_i)^{-1} (\Delta_i - \mu_{n_f}(\theta_i))$.

Given the uncertainty quantification provided by (A.6) and (A.7), if there is a finite set of points, say $\theta_1, \dots, \theta_n$, approximating the Pareto set, with corresponding approximation f_1, \dots, f_n of the Pareto frontier, expected hypervolume improvement (EHVI) measures the volume of the space dominated by the current approximation of the Pareto frontier and bounded below by a reference point, the so-called Pareto hypervolume. EHVI was firstly used as an acquisition function in multi-objective Bayesian optimization by [Emmerich \(2005\)](#), where an expectation of the hypervolume improvement is taken with respect to the surrogate model uncertainty to define the acquisition function. In the MOBOLFI method, multi-objective BO is applied to a vector of expected discrepancies, and the simulated discrepancies are noisy. For this reason, we use the noisy expected hypervolume improvement (NEHVI) ([Daulton, Balandat and Bakshy, 2021b](#)) for the acquisition function. NEHVI implements a Bayesian treatment when calculating EHVI, integrating uncertainty about the Pareto frontier. This makes NEHVI more suitable than EHVI as an acquisition function with noisy data.

[Gutmann and Corander \(2016\)](#) chose the tolerance t in the univariate BOLFI method as the q -quantile of $\Delta_1, \dots, \Delta_{n_f}$, where $q \in (0, 1)$. In the bivariate MOBOLFI method, we extend the choice of tolerance $t = (t_1, t_2)$ to the 2-dimensional vector q -quantile of $\Delta_1, \dots, \Delta_{n_f}$, where $q \in (0, 1)^2$. Given that the evaluation of ABC approximate likelihood involves t , we also did a comparison study over different q -quantile tolerance for 3 different examples, by letting $q = 0.01/0.05/0.1/0.2$. Our visuals present the affect of tolerance on performance of inference, varying by examples.

In multi-objective Bayesian Optimization, one practical difficulty is the scaling of objectives. For a fixed diagonal matrix V , instead of applying multi-objective BO to a vector of noisy discrepancies Δ , we could apply it to $V^{-1}\Delta$ instead, and in general the results are not invariant to the choice of V . [Figure 6](#) studies the effect of scaling on inference in a toy example with $V^{-1} = \text{diag}(w, 1)$, where w is a scalar weight. Since only two objectives involved, we follow the notation in [Section 4.1](#), where $\Delta = (\Delta_1(X^{(i)}, X^o), \Delta_2(W^{(i)}, W^o))$ denotes the joint objective over two data sources X and W . From the figure, we find that with different w , if we simply add the discrepancy to get a univariate discrepancy for the BOLFI posterior the approximate posterior differs markedly, while for MOBOLFI the approximate posterior is less sensitive to w . Not doing scaling is equivalent to setting the $V^{-1} = I_2$, i.e. the red curve in this figure, which is not the choice with the best performance.

One classic scaling method in the machine learning literature is normalization by using Mean absolute deviation (MAD). [Algorithm 1](#) presents the detailed steps of doing scaling

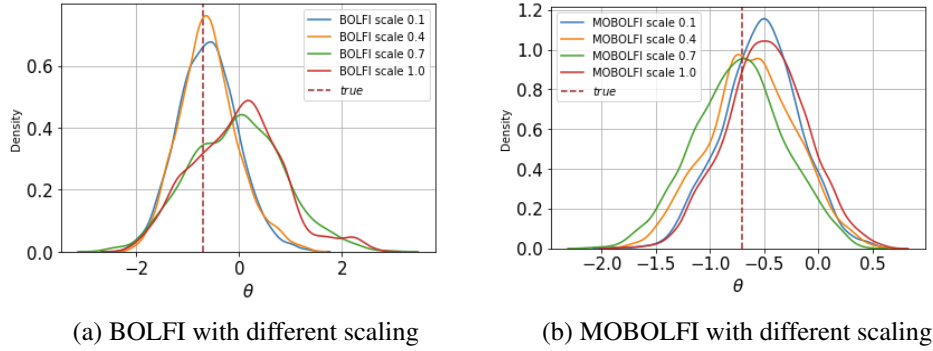


Figure 6: Approximate posterior in the toy example given different scaling weights to Δ_1 . The left column shows the BOLFI approximate posteriors given $weight = 0.1/0.4/0.7/1.0$ scaling, while the training objectives for BO is defined to be $weight * \Delta_1 + \Delta_2$. The right column presents the MOBOLFI approximate posteriors given the same scaling.

of a joint noisy objective Δ for implementing BOLFI. The key idea of Algorithm 1 is to put each elements of Δ on a similar scale. The use of Algorithm 1 does not always result in the best performance. In the plot 6a, the green curve with $w = 0.7$ is chosen by Algorithm 1 (rounding to 1 decimal places). The scaling with best performance is example specific, depending on the information of each data source, the LFI method and the BO acquisition function. We leave further investigation of optimal scaling approaches to future work. For the results of this paper, by default we choose the scaling as the outcome (rounded to 1 decimal places) from algorithm 1 using $n = 100$. The auxiliary model example (orange curve in Figure 11) defines a discrepancy as the score vector of an auxiliary model, and the scaling in this example is slightly different and will be discussed in Section C.3 of this supplement.

Algorithm 1 Scaling of discrepancies in (MO)BOLFI

Require: Prior $\pi(\cdot)$ of θ , target function $\Delta = (\Delta_1, \dots, \Delta_K)^T$ to scale, number of sample size n
 Sample $\theta^{(i)} \sim \pi(\theta), i = 1, \dots, n$
 For each θ_i , evaluate the corresponding target function $\Delta(\theta^{(i)}) = (\Delta_1(\theta^{(i)}), \dots, \Delta_K(\theta^{(i)}))^T$
 For $j = 1, \dots, K$, write $v^{(j)} = \text{MAD}\{\Delta_j(\theta^{(1)}), \dots, \Delta_j(\theta^{(n)})\}$
 Write $V = \text{diag}(v^{(1)}, \dots, v^{(K)})$
 Scale the target function $\Delta_{\text{scale}} = V^{-1}\Delta$
 (In BOLFI, $\Delta = \Delta_1 + \dots + \Delta_K$, and the scaled discrepancy is $\Delta_{\text{scale}} = V_{11}^{-1}\Delta_1 + \dots + V_{KK}^{-1}\Delta_K$)

B. Experiment setup and extra findings - Toy example. We give some further details of the implementation of MOBOLFI and some additional experiments that were not included in the main text due to space limitations. Code to implement all experiments can be obtained at <https://github.com/DZCQs/Multi-objective-Bayesian-Optimization-Likelihood-free-Inference-MOBOLFI.git>.

B.1. Experiment setup - toy example. In the toy example in the main text initial training data of 100 observations was used, and BOLFI/MOBOLFI was used to train 1-dimensional/2-dimensional surrogate GP models respectively with 200 BO acquisitions. Parameter samples are drawn from the approximate posterior distribution (Section 2.3) using Hamiltonian Monte Carlo (HMC) with tolerance t set to be the 1% quantile of the training data discrepancies.

This is done element-wise for each discrepancy to get the vector of tolerances for MOBOLFI. We implement HMC using the hamiltorch package (Cobb and Jalaian (2021)), running four chains for 8,000 iterations each, using step size 0.1 and one step within each proposal (which corresponds to a Metropolis-Hastings adjusted Langevin algorithm).

For MOBOLFI, the objective function optimized is

$$D(\theta) = (E(\Delta_1(X, X^o)), E(\Delta_2(W, W^o)))^\top,$$

where X is the synthetic data and X^o is the observed data for the first data source, $\Delta_1(X, X^o)$ is the discrepancy for the first data source, W is synthetic data and W^o is the observed data for the second data source, and $\Delta_2(W, W^o)$ is the discrepancy for the second data source. The definition of the discrepancies is given in the main text. For implementing BOLFI, the training data is $\{\theta_i, w \cdot \Delta_1(X^{(i)}, X_o) + \Delta_2(W^{(i)}, W_o)\}_{i=1}^{100}$, where $w = 0.4$ is the scaling with best performance from a number of alternatives (see figure 6a in Section A.3 of this supplement). We use the lower confidence bound acquisition function for BOLFI with $\eta = 0.1$ in eq. A.4. For implementing MOBOLFI, the training data is $\{\theta_i, (w \cdot \Delta_1(X^{(i)}, X_o), \Delta_2(W^{(i)}, W_o))\}_{i=1}^{100}$. We use the NEHVI acquisition function (Daulton, Balan-dat and Bakshy, 2021b) with a reference point $\min_i((\Delta_1(X^{(i)}, X_o), \Delta_2(W^{(i)}, W_o))) - 0.1$. Each optimization in the multi-objective BO iterations approximates the optimum of the acquisition function from 100 candidate samples in 10 restarts. To avoid observations with discrepancy values which are too large (which affects GP training), we set a mild rejection criterion to filter out observations higher than a threshold, i.e. the 99%-quantile (rounded to 1 decimal places) obtained from simulated discrepancies that are drawn without any filtering criterion.

The botorch package maximizes the supplied objective function by default, and so in implementation of BOLFI we maximize the negative expected discrepancy. Gutmann and Corander (2016) minimizes the lower confidence bound as (A.4) in their work, and when maximizing the negative expected discrepancy it is equivalent to use the upper confidence bound as acquisition function,

$$(B.1) \quad A_n(\theta) = \mu_n(\theta) + \sqrt{\eta_n^2 \sigma_n^2(\theta)}.$$

B.2. Extra findings - toy example. In addition to the experiments in the main text, Figure 7 shows MOBOLFI approximate posteriors of θ_1 for different choices of the number of iterations in the BO algorithm and for different choices of tolerance. The approximate posteriors are kernel density estimates from HMC samples. The left-hand column of the figure demonstrates that the MOBOLFI approximate posterior variance decreases with more BO iterations. This is expected, since the surrogate model uncertainty contributes to the uncertainty in the MOBOLFI approximate posterior. The right-hand column of the figure demonstrates that the MOBOLFI approximate posterior is closer to the true posterior when a smaller quantile of the training data is used for the tolerance. In Figure 7 (b), 200 BO acquisitions were used. Gutmann and Corander (2016) suggested using the 5% quantile of the training data, but a 1% quantile attains comparable performance in this example. Both the selection of tolerance levels in the likelihood approximation and the number of BO iterations used are crucial for achieving accurate approximate posterior distributions using MOBOLFI.

MOBOLFI differs from BOLFI by using multiple discrepancies in the BO algorithm. To explore the sensitivity of inference to including multiple data sources when the model for some data sources does not depend on some parameters, we modify the simulator as follows. The first 8 elements of θ_{true} are shared by both X and Y. However, the 9th element of θ_{true}

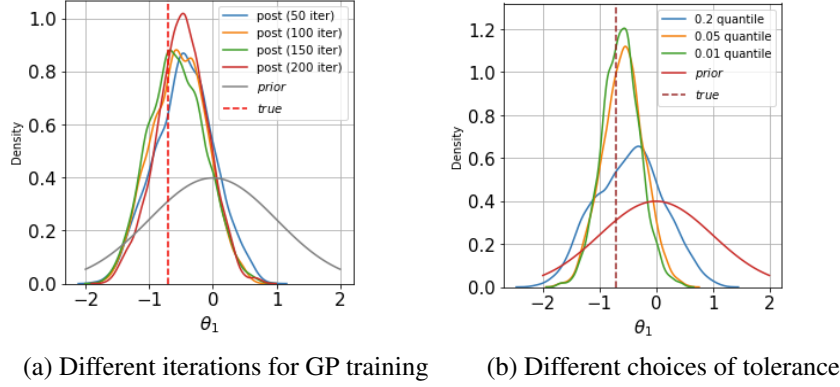


Figure 7: Approximate posterior for the toy example given different numbers of training iterations and tolerances. The left column shows the MOBOLFI approximate posteriors given 50/100/150/200 BO iterations. The right column presents the approximate posteriors for threshold t set to 20%/5%/1% quantiles of the training data discrepancies. All approximate posterior densities are kernel density estimates from HMC samples. The red dashed line is at $\theta_1^{\text{true}} = -0.7$

contributes to X only, and the 10th element of θ_{true} contributes to Y only. Specifically,

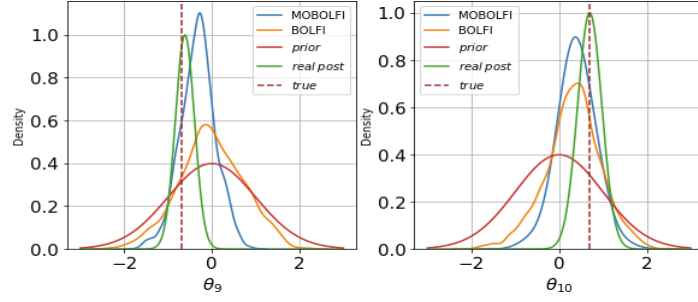
$$\begin{aligned}
 \theta &\sim \mathbb{N}(\theta|0, I) \\
 X_n &\sim \mathbb{N}(x|\theta, I), n = 1, \dots, N \\
 w(t) &= \theta dt + \sigma dW(t) \\
 \theta_X &= (\theta_{\text{true},1}, \dots, \theta_{\text{true},8}, \theta_{\text{true},9})^T \\
 \theta_W &= (\theta_{\text{true},1}, \dots, \theta_{\text{true},8}, \theta_{\text{true},10})^T
 \end{aligned}
 \tag{B.2}$$

We apply MOBOLFI with the same experiment setup as in Section B.1 of this supplement. The MOBOLFI and BOLFI approximate posteriors are presented in Figure 8. We focus on the parameters θ_9, θ_{10} , which are parameters influencing the distribution of only one of the data sources. In plot 8a, the MOBOLFI approximate posterior, leveraging correlated noise between data sources, still outperforms BOLFI in inference of θ_9, θ_{10} . In plot 8b, for θ_{10} not depending on X , the MOBOLFI approximate posterior conditional on of X does not obtain smaller variance than the BOLFI approximate posterior. That is not surprising to see, since information from X is viewed as useless and redundant for inference of θ_{10} . On the other hand, MOBOLFI still performs better than BOLFI in the inference of θ_9 . Plot 8c shows that approximate MOBOLFI posterior conditional on W only does not obtain smaller variance than the BOLFI approximate posterior, for θ_9 not depending on W .

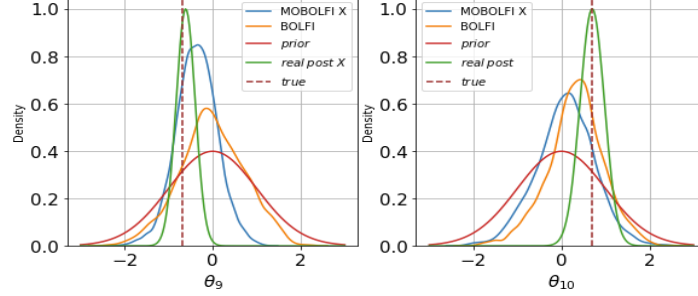
C. Experimental setup and extra findings: MLBA example.

C.1. *MLBA closed form likelihood function.* Consider decision-making for a single individual first. For a drift rate $v_a \sim N(d_a, s^2)$, $a = 1, \dots, M$, the probability density function (pdf) of the time t taken for the accumulator a to reach the threshold χ is (see Brown and Heathcote (2008), Appendix A for a derivation):

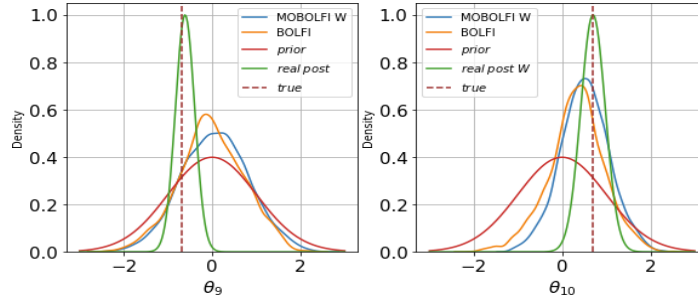
$$f_a(t) = \frac{1}{\mathcal{A}} \left[-d_a \Phi \left(\frac{\chi - \mathcal{A} - td_a}{ts} \right) + s\phi \left(\frac{\chi - \mathcal{A} - td_a}{ts} \right) + d_a \Phi \left(\frac{\chi - td_a}{ts} \right) - s\phi \left(\frac{\chi - td_a}{ts} \right) \right],
 \tag{C.1}$$



(a) MOBOLFI vs BOLFI



(b) Information in X



(c) Information in W

Figure 8: Approximate posterior for the updated toy example with two parameters θ_9, θ_{10} solely depending on two data sources X, W , respectively. The row 8a shows the MOBOLFI and BOLFI approximate posteriors under the updated simulator, colored by blue/orange. The green curve is the real posterior, the red curve is the prior and the dash red line is the true value of θ_9, θ_{10} . In row 8b/8c the MOBOLFI and BOLFI approximate posteriors calculated by marginal likelihood of X/W are given by blue/orange lines. The green curve is the real posterior of X/W respectively.

where $\phi(\cdot)$ and $\Phi(\cdot)$ are the pdf and cdf of the standard normal distribution.

Its associated cumulative density function (cdf) is:

$$\begin{aligned}
 (C.2) \quad F_a(t) &= 1 + \frac{\chi - \mathcal{A} - td_a}{\mathcal{A}} \Phi\left(\frac{\chi - \mathcal{A} - td_a}{ts}\right) - \frac{\chi - td_a}{\mathcal{A}} \Phi\left(\frac{\chi - td_a}{ts}\right) \\
 &\quad + \frac{ts}{\mathcal{A}} \phi\left(\frac{\chi - \mathcal{A} - td_a}{ts}\right) - \frac{ts}{\mathcal{A}} \phi\left(\frac{\chi - td_a}{ts}\right).
 \end{aligned}$$

The joint pdf of $CH = a$ and $RT = t + \tau_0$ is

$$(C.3) \quad \text{MLBA}_{\text{joint}}(CH = a, RT = t + \tau_0) = f_a(t) \prod_{b \neq a} (1 - F_b(t)),$$

and the marginal pdf of $CH = a$ is

$$(C.4) \quad \text{MLBA}_{\text{choice}}(CH = i) = \int_0^\infty f_a(t) \prod_{b \in \mathcal{C}, b \neq a} (1 - F_b(t)) dt,$$

where \mathcal{C} is the choice set.

We follow the adjustment suggested by [Terry et al. \(2015\)](#), where the drift rate follows a truncated normal distribution: $v_a \sim TN(d_a, s^2, 0, \infty)$, with 0 and ∞ as lower and upper bounds of the support. This distribution helps correct the original pdf and cdf in eq.C.1 and eq.C.2. Moreover, the truncated normal distribution resulted in superior performance in empirical experiments conducted by [Hancock et al. \(2021b\)](#). Therefore, both $f_a(t)$ and $F_a(t)$ are additionally divided by a factor $\Phi(\frac{d_a}{s})$ in eq.C.1 and eq.C.2.

C.2. Experimental setup - MLBA. When working on synthetic data, we firstly construct a training dataset $\{\theta^{(i)}, (RT^{(i)}, CH^{(i)})\}_{i=1}^{100}$ of 100 observations. In BOLFI/MOBOLFI, a univariate/bivariate GP is trained with 1000 iterations. Likelihood approximations for BOLFI/MOBOLFI use tolerance t given by the 1% quantile of the training discrepancies, and samples were generated from the approximate posterior distributions using De-MCMC. These samples are compared to samples from the posterior with the closed form likelihood C.3 above.

For MOBOLFI, the objective function optimized is

$$D(\theta) = (E(\Delta_1(RT, RT^o)), E(\Delta_2(CH, CH^o)))^\top,$$

where RT, CH are synthetic response time and choice data respectively, RT^o and CH^o are the corresponding observed data, $\Delta_1(RT, RT^o)$ is the discrepancy for the response time data and $\Delta_2(CH, CH^o)$ is the discrepancy for the choice data. The definition of the discrepancies is given in the main text. In BOLFI, the training objective is $w \cdot \Delta_1(RT, RT^o) + \Delta_2(CH, CH^o)$, where $w = 0.7$. In MOBOLFI, the training objective is the 2-dimensional vector $(w \cdot \Delta_1(RT, RT^o), \Delta_2(CH, CH^o))$. In BOLFI, the acquisition function is defined to be the Lower Confidence bound with variance weight $\eta = 0.1$ defined in eq.A.4. In MOBOLFI the Bayesian Optimization acquisition function is chosen to be the qNEHVI (see https://botorch.org/api/acquisition.html#botorch.acquisition.multi_objective.monte_carlo.qNoisyExpectedHypervolumeImprovement for details). Both MOBOLFI and BOLFI surrogate models are trained with 1000 BO acquisitions.

For faster convergence, we set different hyperparameters for running De-MCMC to sample from MOBOLFI/BOLFI and the posterior with closed form likelihood. When sampling from the posterior for closed form likelihood, we set 9 chains, sample size 20000, burn-in size 18000 and migration rate 0.5. When sampling from BOLFI/MOBOLFI approximate posteriors, we set 9 chains, sample size 16000 and burn-in 13000. The coefficient γ in the De-MCMC algorithm is set to be the fixed constant $2.38/\sqrt{2 \cdot n_\theta}$, where $n_\theta = 6$ is the number of parameters we infer.

Similar to the toy example, we set some rejection criteria in sampling the initial training set for BO. Points with values of any one of the discrepancies greater than a threshold, i.e. the 99%-quantile obtained from simulated discrepancies that are drawn without any filtering criterion, are discarded. In MLBA simulation we observe that there are some prior samples $\theta^{(i)}$ that simulate $RT^{(i)} = \{RT_1^{(i)}, \dots, RT_{320}^{(i)}\}$ where $RT_j^{(i)} \approx \overline{RT^o}, \forall j \in \{1, \dots, 320\}$, where $\overline{RT^o}$ denotes the sample mean of RT^o . Ideally the prior should be constrained to avoid such degenerate regions of the parameter space, but these regions are not easily characterized analytically. Hence we also filter out $\theta^{(i)}$ such that $\text{Var}(RT^{(i)}) < \text{Var}(RT^o) \cdot 0.7$.

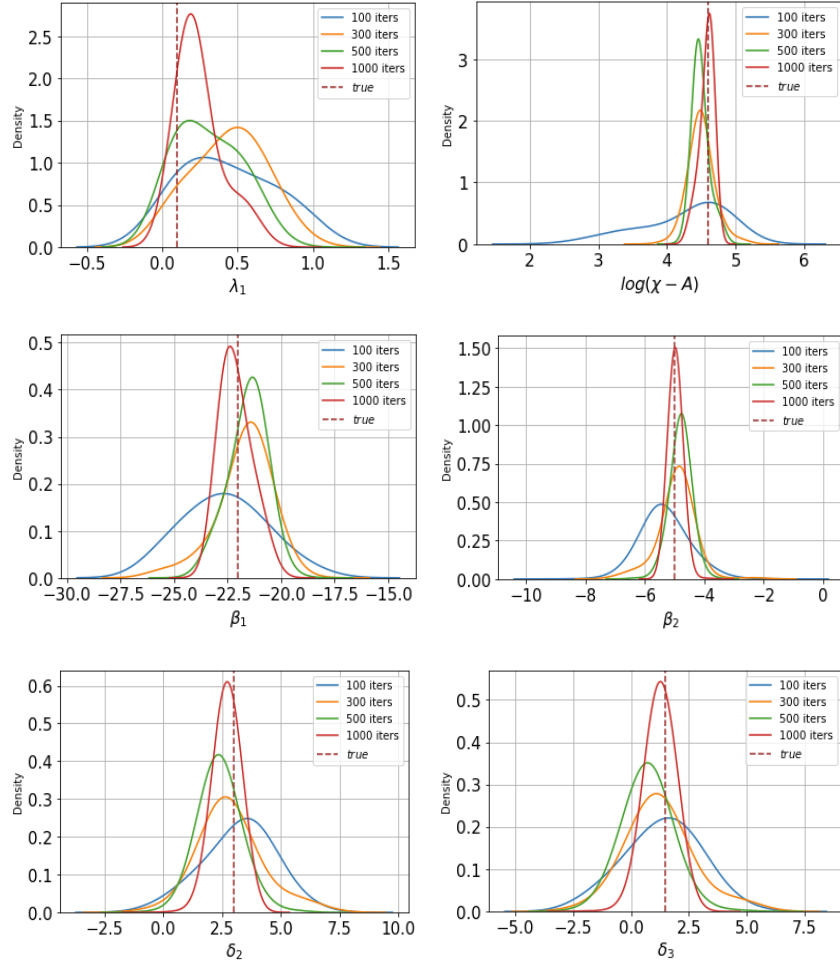


Figure 9: Approximate posteriors for MLBA example given different numbers of iterations for the BO algorithm. Each plot shows approximate marginal posteriors for one parameter of interest. The densities shown are kernel density estimates obtained from MCMC samples. The dashed red line shows the location of the corresponding true parameter.

C.3. Extra findings - MLBA example (Synthetic data). Similar to the toy example, we build MOBOLFI approximate posteriors given different number of iterations for the BO algorithm. Figure 9 compares kernel density estimates obtained from samples from the approximate posteriors. Due to the complexity of the MLBA simulator, we need many more iterations in the BO algorithm than for the toy example to obtain good approximations. The Figure shows that 100 iterations in the BO algorithm is too little, but the approximation to the marginal posteriors has mostly stabilized after 300 iterations for most parameters.

We also investigate the affect of tolerance t on MOBOLFI performance in MLBA. In Figure 10, we compare the MOBOLFI approximate posteriors for tolerances specified as 10%/5%/1% quantiles of the training discrepancies. Given enough BO iterations, the 1% quantile is the best choice. Although the performance of MOBOLFI is sensitive to the choice of t , setting the tolerance to a 1% or 5% quantile of the training data works well across many problems.

When a summary statistic is used in the definition of the discrepancy, its choice is another factor that affects the performance of MOBOLFI. For summary statistic based LFI methods,

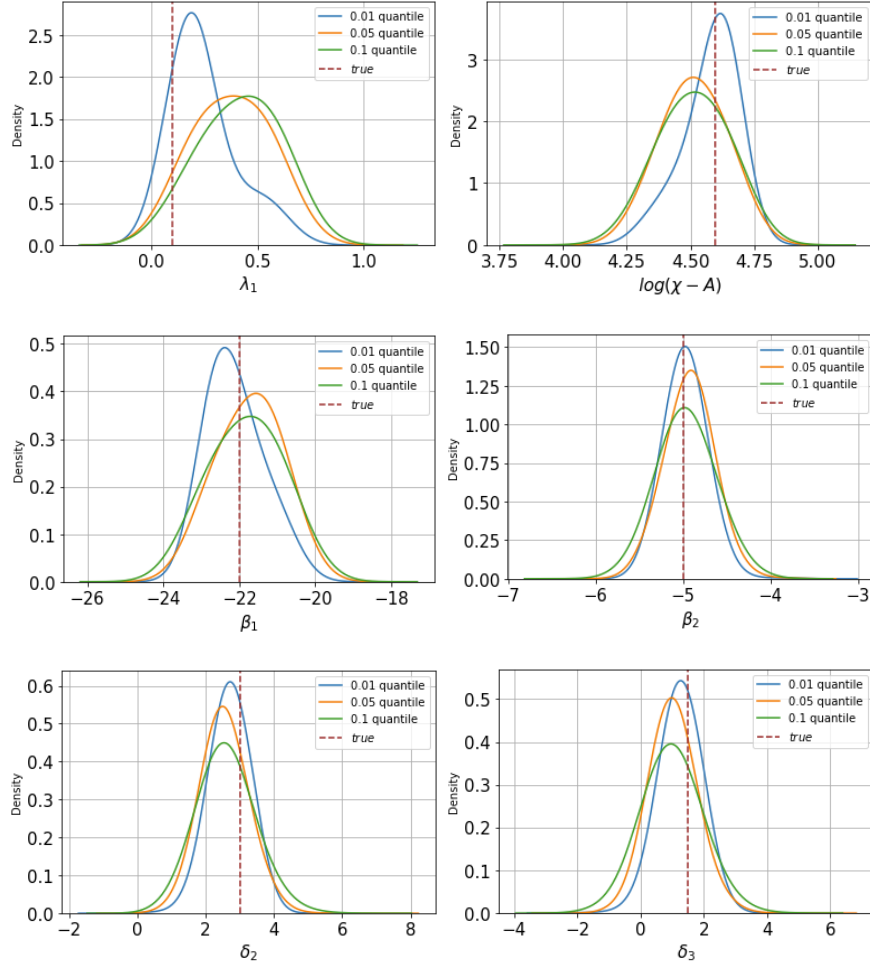


Figure 10: Approximate posteriors of MLBA example given different levels of quantile of training dataset as the tolerance t . The blue/orange/green curve represents the MOBOFBI approximate posterior (with 1000 iterations training) using 10%/5%/1% quantile of the training dataset as the tolerance t respectively. The dashed red line shows the location of the true parameter.

the choice of summary is important, because good summaries can reduce the computational burden with little loss of information. In Figure 11, we evaluate MOBOFBI approximate posteriors obtained using two approaches. The first approach uses the discrepancies discussed in the main text. The second approach changes the discrepancy used for the choice data, by defining summary statistics using an auxiliary model (e.g., [Drovandi, Pettitt and Lee, 2015](#)). Specifically, we adopt the score vector evaluated at the maximum likelihood estimate (MLE) for the observed data for a multinomial logit (MNL) model as the choice data discrepancy.

To explain further, the MNL model is a discrete choice model based on random utility maximization theory ([McFadden, 1974](#)). In the MNL, the choice probability for the alternative a is

$$(C.5) \quad P_a = \frac{\exp(V_a)}{\sum_b \exp(V_b)}$$

where V_a is a systematic utility of the alternative a , represented by a set of attributes $X = (X_1, \dots, X_K)$ and corresponding parameters $\xi = (\xi_1, \dots, \xi_K)$, where K is the total number of parameters. Since it has a closed-form likelihood function, the parameters can be estimated by maximum likelihood estimation. Write $p_A(CH; \xi)$ for the likelihood for the MNL auxiliary model for choice data CH and parameter ξ . The score function is $S_A(CH; \xi) = \nabla_{\xi} \log p_A(CH; \xi)$. Writing CH^o for the observed choice data, and $\hat{\xi}$ for the MLE for the observed choice data, we have $S_A(CH^o; \hat{\xi}) \approx 0$, and for simulated choice data CH we use as summary statistics $S_A(CH; \hat{\xi})$ (i.e. we use the $(K \times 1)$ score vector for the data CH evaluated at the MLE $\hat{\xi}$ for the observed choice data as the vector of summary statistics).

Each component of the score vector has a different scale from the others because the parameters ξ correspond to different scales of attributes (e.g., driving range and purchase price). Therefore, the score vector $S_A(CH; \hat{\xi})$ should be converted into a scalar value to be used as choice data discrepancy $\Delta_2(CH, CH^o)$. We scale parameter-specific components of the score vector to put all components on a similar scale as follows. Sample from the prior $\theta^{(i)} \sim \pi(\theta)$, $i = 1, \dots, n$. For each i , we evaluate the corresponding score vector $S^{(i)} = S_A(CH^{(i)}; \hat{\xi})$, where $CH^{(i)}$ is the choice data simulation given $\theta^{(i)}$. Then, we apply Algorithm 1 to obtain the scaling weight V_1^{-1} of the parameter-specific K-components of the score vectors with sample size $n = 100$ and target function $S_A(\cdot; \hat{\xi})$. Finally, the choice data discrepancy is defined as $\Delta_2(CH, CH^o) = V_1^{-1} S_A(CH; \hat{\xi})$.

To implement the MOBOLFI approach, we need to calculate the training objective by calculating two data source-specific discrepancies. The response data discrepancy is the one used in the main text, and the joint discrepancy is $(\Delta_1(RT, RT^o), V_2^{-1} \Delta_2(CH, CH^o))$ where V_2^{-1} is obtained by Algorithm 1.

In our experiment, we generated $n = 100$ MLBA datasets for $K = 5$ parameters of the MNL auxiliary model and obtained $V_1^{-1} = (128.4, 226.2, 1656.6, 519.9, 2269.1)$ and $V_2^{-1} = 0.0007$, respectively.

In Figure 11, we compare MOBOLFI using the choice discrepancy from the main text with the auxiliary model choice discrepancy (MOBOLFI AUX). The closed-form likelihood (MLBA) is used as a benchmark model. Given enough training, the MOBOLFI and MOBOLFI AUX show different advantages in approximating the posterior with regard to point estimate and posterior variance. The lower posterior variance indicates more robust estimates, while the point estimate closer to the true parameter indicates accuracy for decision-making in practice (e.g., an estimate of electric vehicle adoption rate in this MLBA case). Since the MLBA parameters are behaviorally related to both reaction time and choice decision, the MOBOLFI AUX affects all parameters. For λ_1 , β_1 , and $\log(\chi - \mathcal{A})$, the MOBOLFI AUX outperforms the MOBOLFI by providing a slightly better point estimate while reducing posterior variance in parameter inference, indicating the validity of adopting summary statistics based on an auxiliary model. For β_2 , δ_2 , and δ_3 , the approximate posterior distributions from the MOBOLFI are superior to those from MOBOLFI AUX with similar posterior variance but much better point estimates. This result suggests that the performance of MOBOLFI and MOBOLFI AUX are comparable.

C.3.1. Misspecified MLBA. In the main text we have argued that including response time data in addition to choice data improves parameter estimation for the MLBA model. We now consider a situation involving misspecification, and illustrate the advantages of MOBOLFI in detecting conflict between different parts of the data. We adjust the experimental setup by defining two sets of parameters $\theta_{RT}^{\text{true}} = (0.2, -25, -3.5, 6, 4, \log(99))$ and $\theta_{CH}^{\text{true}} = (0.05, -24, -6.5, 3, 1.5, \log(199))$ for simulating response time and choice data respectively.

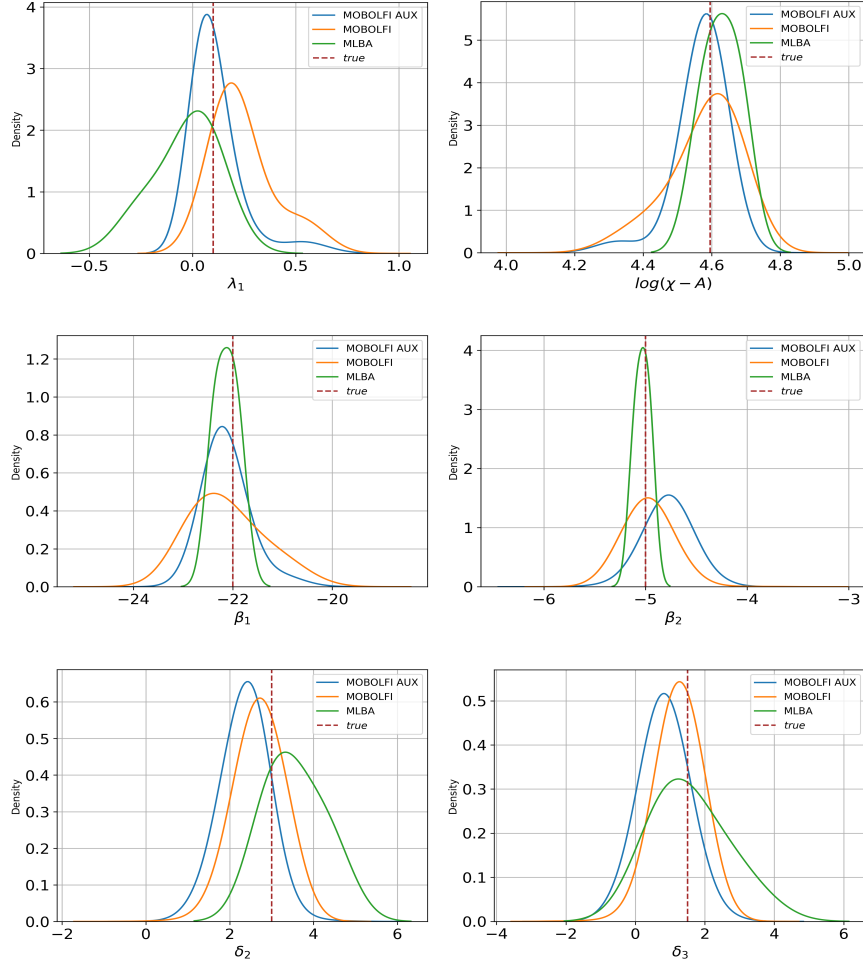


Figure 11: Approximate posteriors of MLBA example estimated by different data summary for response choice. The blue and orange curves represent the MOBOLFI approximate posterior (with 1000 iterations training) using the original distance (MOBOLFI) and score function of an auxiliary model (MOBOLFI AUX) as the data summary, respectively. The red dash line is the value of true parameter θ^{true} .

We simulate data (RT^{rt}, CH^{rt}) by MLBA taking $\theta_{RT}^{\text{true}}$ as input, data (RT^{ch}, CH^{ch}) by MLBA taking $\theta_{CH}^{\text{true}}$ as input. The synthetic observed data $(RT^o, CH^o) = (RT^{rt}, CH^{ch})$ concatenates the response time data generated using $\theta_{RT}^{\text{true}}$ and the choice data simulated using $\theta_{CH}^{\text{true}}$. Therefore, the two data sources provide conflicting information about the parameter vector.

We follow the same design as in Appendix 3.2 with some minor changes. Firstly, we remove the criteria that filters out points with values of any one of the discrepancies greater than the 99%-quantile obtained from simulated discrepancies that are drawn without any filtering criterion. This is done because, with conflicting information, parameter samples are likely to obtain low value of discrepancy on one data source and high value on the other. Secondly, the number of iterations for the BO algorithm is set to be 500.

Applying MOBOLFI to such (RT^o, CH^o) , we claim that the Bayesian Optimization explores a range of local optimum points (including $\theta_{RT}^{\text{true}}$ and $\theta_{CH}^{\text{true}}$), in terms of minimizing $E((\Delta_1, \Delta_2))$. Although we cannot observe the expected discrepancy, Figure 12 shows the

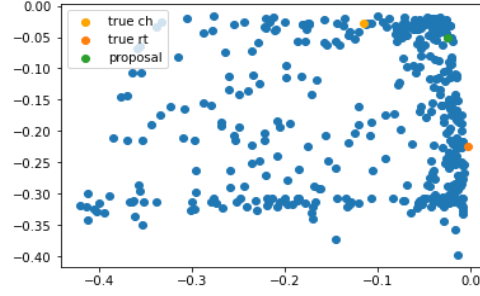


Figure 12: Noisy Negative discrepancy values of Bayesian Optimization acquisition points. The horizontal axis denotes the negative RT discrepancy, the vertical axis denotes the negative CH discrepancy. The discrepancies have been scaled to a similar range. The yellow/orange point represents simulated discrepancies obtained using $\theta_{RT}^{\text{true}}/\theta_{CH}^{\text{true}}$ as input. The green point is a simulated vector of negative discrepancies obtained at the mode of the MOBOLFI approximate posterior.

noisy negative discrepancy values of Bayesian Optimization acquisitions. Besides $\theta_{RT}^{\text{true}}$ and $\theta_{CH}^{\text{true}}$, the points in the top-right corner of the plot, i.e. in the region around the green point, obtain discrepancy values close to 0. With high probability, the expected negative discrepancy of these points are no smaller than that of either $\theta_{RT}^{\text{true}}$ or $\theta_{CH}^{\text{true}}$ on at least one data source. Points in the top-right corner suggest that, with respect to randomness of noise, MOBOLFI is able to deal with the complexity of conflicting information from multi-source data, acquiring all the local optimum points that minimize the expected discrepancy given enough iterations for training.

MOBOLFI approximate posteriors of these parameters under misspecification are shown in Figure 13. For λ_1 , both data sources contribute to the inference, and the posterior calculated using single data sources are similar to the posterior calculated by the joint likelihood. For $\log(\chi - \mathcal{A})$, the definition of χ determines that inference of it mainly depends on the response time data RT . It is unsurprising to see that the posterior calculated by the joint likelihood has similar location to the posterior calculated conditional on RT only. The posterior calculated conditional on CH only provides much less information, having a large variance. For β_1 , the true values for the different data sources lie in the tail of the posterior calculated using the joint likelihood, while the posterior calculated conditioning on only one data source are similar and consistent with the true values from both data sources. As discussed above, there is a set of local optimum points that could obtain similar performance in evaluating the discrepancy to $\theta_{RT}^{\text{true}}$ and $\theta_{CH}^{\text{true}}$. The marginal approximate posterior of β_1 calculated by the joint likelihood puts weight on points other than $\theta_{RT}^{\text{true}}$ and $\theta_{CH}^{\text{true}}$ consistent with the data. For β_2 , we found the posterior calculated using the joint likelihood is closer to the posterior calculated conditioning only on the CH data but with variance larger. This differs from the behaviour for β_1 . We believe this is because given the fixed $\beta_3 = -6$, the values of β_2 in $\theta_{RT}^{\text{true}}$ and $\theta_{CH}^{\text{true}}$ are close to the value of β_3 but away from β_1 . This suggests that in the synthetic data example, attribute 1 is more important in evaluating evidence of alternatives which directly affects the response time. It is not surprising then to see that β_2 measures influence of the less important attribute 2 and appears to be more sensitive to the choice data CH than β_1 . For δ_2 and δ_3 , the alternative specific constant is added into the drift rate mean calculation directly, unrelated to the attribute pairwise-comparison, which is the main source of variation of drift rate mean. Therefore, the posterior calculated using the joint likelihood appears similar to the posterior calculated conditional on CH only. Inference of δ_2 and δ_3 should mainly depend on the CH data. However, we do observe that the conflicting information from RT does brings

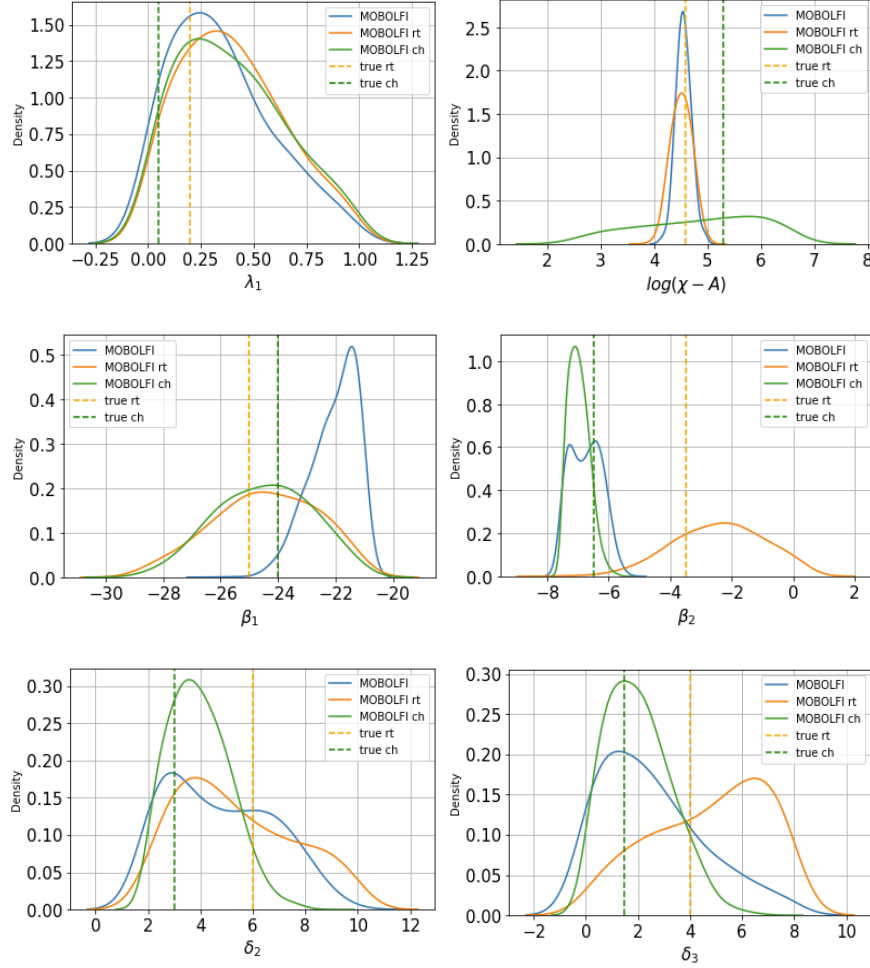


Figure 13: Approximate marginal posteriors for MLBA example under mis-specification. The blue curve represents the MOBOLFI approximate posterior calculated using the joint likelihood of two data sources. The orange/green curve are the MOBOLFI approximate posteriors calculated by the approximate likelihood of RT/CH data only. The orange/green dash line shows the location of the true parameters in $\theta_{RT}^{\text{true}}$ and $\theta_{CH}^{\text{true}}$.

more uncertainty to the approximate posterior calculated by joint likelihood, which shows larger variance than the approximate posterior calculated conditional on CH only.

C.4. Extra findings - MLBA example (empirical case).

C.4.1. MLBA variants selection. In the main text,

$$\theta = (\lambda_1, \delta_{ICEV}, \log \beta_{TC}, \log \beta_{\log DR}, \log(\chi - \mathcal{A}))$$

is estimated fixing $\lambda_2 = 0$. Theoretically, λ_2 is also estimable. Table 1 here provides more justification for selecting the $\lambda_2 = 0$ MLBA variant for further study on MOBOLFI. For MLBA variant with free λ_2 , its MAP value is very close to 0. Fixing $\lambda_2 = 0$ not only reduces the number of estimable parameters but brings a slightly higher log-likelihood.

TABLE 1
Closed-form parameter estimate based on two MLBA variants.

parameter	$\lambda_2 = 0$		λ_2 is free	
	posterior mean (sd)	posterior MAP (95% HDI)	posterior mean (sd)	posterior MAP (95% HDI)
$\log \beta_{TC}$	2.055 (0.106)	2.082 (1.848 , 2.264)	2.179 (0.145)	2.068 (1.911 , 2.462)
$\log \beta_{\log DR}$	1.141 (0.175)	1.128 (0.814 , 1.49)	1.438 (0.533)	1.116 (0.893 , 2.701)
δ_{ICEV}	0.431 (0.401)	0.55 (-0.369 , 1.145)	-0.005 (0.802)	0.511 (-1.712 , 1.114)
λ_1	0.199 (0.05)	0.203 (0.115 , 0.306)	0.196 (0.041)	0.202 (0.132 , 0.29)
λ_2	-	-	0.073 (0.053)	0.001 (0 , 0.167)
$\log(\chi - \mathcal{A})$	0.705 (0.12)	0.752 (0.463 , 0.921)	0.689 (0.121)	0.73 (0.452 , 0.918)
Log-likelihood	-2507.614	-2507.52	-2509.831	-2509.107

C.4.2. *Results with other discrepancy design.* In the main text, we used an average of 1-Wasserstein distance over $S = 30$ simulated datasets for RT discrepancy Δ_1^* and Brier Score for CH discrepancy Δ_2^* for the empirical data experiment. As stated there, the chosen discrepancies are more stable and informative compared to those based on a single model simulation, Δ_1 and Δ_2 . Figure 14 shows the MOBOLFI posterior comparison for two different discrepancy designs. According to De-MCMC sampling of the posterior, Δ_1 and Δ_2 (eq.4.4 and 4.5 in the main text) bring larger uncertainty to the posterior compared to Δ^* . Admittedly, there is a trade-off between discrepancy computation speed (Δ^* takes S times as much time as Δ does for the same number of BO acquisitions) and the number of BO acquisitions required for good likelihood approximation. Overall, Δ^* offers a quicker convergence for MOBOLFI training and smaller uncertainty in its approximate posteriors.

C.4.3. *Weak dependence of discrepancies on β and λ_1 .* Figure 15 shows histograms of 1000 discrepancies for simulation data generated by both MOBOLFI and closed-form MAPs. Data generated by two MAPs results in similar distributions of discrepancies, despite closed-form MAP has values of $\log \beta_{TC}$, $\log \beta_{\log DR}$ and λ_1 far from MOBOLFI MAP. This indicates that with appropriately selected δ_{ICEV} and $\log(\chi - \mathcal{A})$, the discrepancies (and the corresponding MLBA simulation) in this experiment are insensitive to $\log \beta_{TC}$, $\log \beta_{\log DR}$ and λ_1 .

To further investigate the effect of $\log \beta_{TC}$, $\log \beta_{\log DR}$ and λ_1 , a sensitivity analysis is done to evaluate changes on discrepancies depending on change on each parameter. Figure 16 demonstrates the discrepancy values over each parameter domain when others are fixed to the MOBOLFI MAP. For each parameter 14 points are selected, of which one is the MAP value and the other 13 are boundaries and its 0.1 neighbour points for 5 equally divided segments over the domain. Take δ_{ICEV} as an example, $\{-3, -2.9, -1.1, -1, -0.9, 0.56, 0.9, 1, 1.1, 2.9, 3, 3.1, 4.9, 5\}$ are selected while 0.56 is the MAP value, $\{-3, -1, 1, 3, 5\}$ are the boundaries of five equal segments over domain $[-3, 5]$ and the rest are associated 0.1 neighbor points within the domain. For each parameter, 100 independent replicates of discrepancy calculation are presented in boxplots. Compared to δ_{ICEV} and $\log\{\chi - \mathcal{A}\}$, $\log \beta_{TC}$, $\log \beta_{\log DR}$ and λ_1 have a weak impact on discrepancies when values of them vary dramatically over the domain. This claims that with appropriately

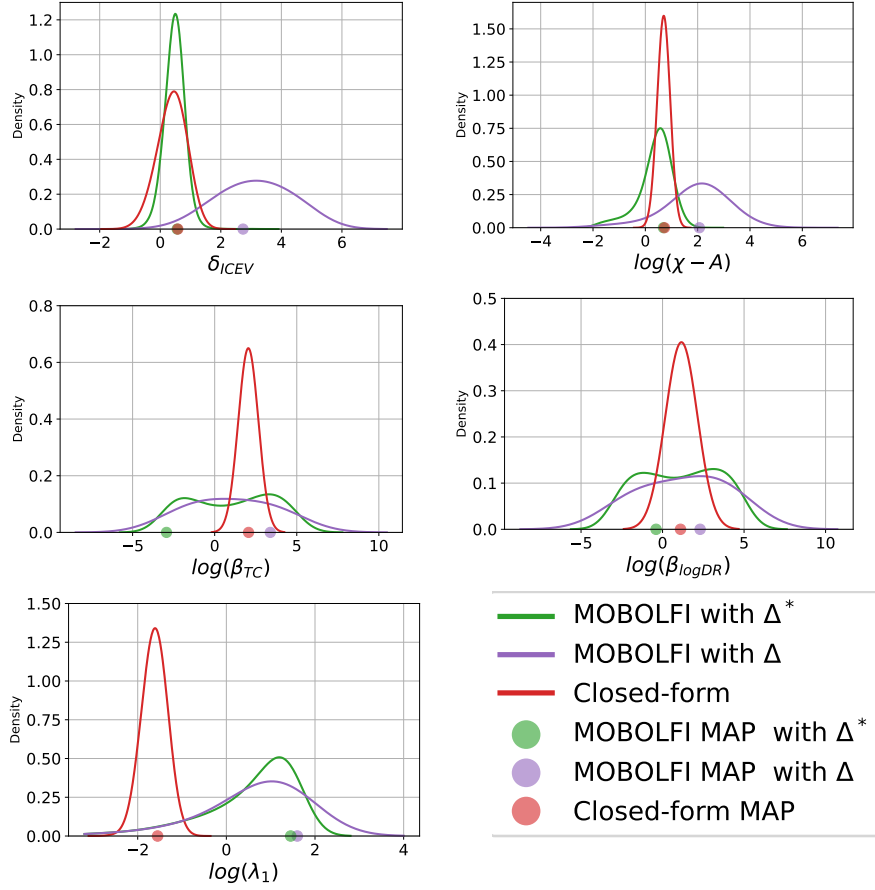


Figure 14: Approximate posteriors of MOBOLFI with different discrepancy designs. The dashed line stands for the MOBOLFI with discrepancy design Δ the same as the synthetic data example. Green is the joint approximate posterior for both CH and RT data, while orange and blue stands for the marginal posterior by RT/CH data only.

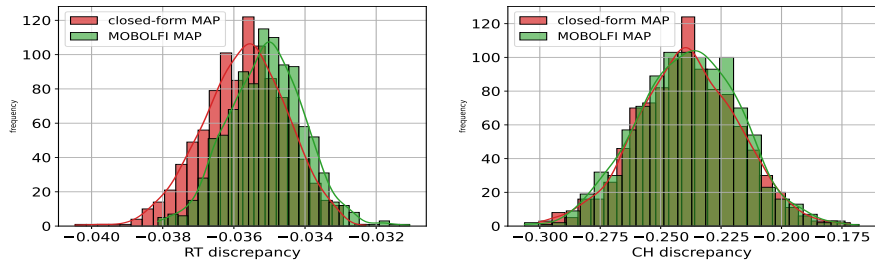


Figure 15: Discrepancy distributions for MAPs over 1000 repetitions (MOBOLFI MAP is in green and closed-form MAP is in red, respectively). The MAPs are selected with the largest (approximated) posterior value among all De-MCMC samplers for posterior estimation.

selected δ_{ICEV} and $\log(\chi - A)$, the discrepancies (and the corresponding MLBA simulation) in this experiment weakly depend on $\log \beta_{TC}$, $\log \beta_{\log DR}$ and λ_1 .

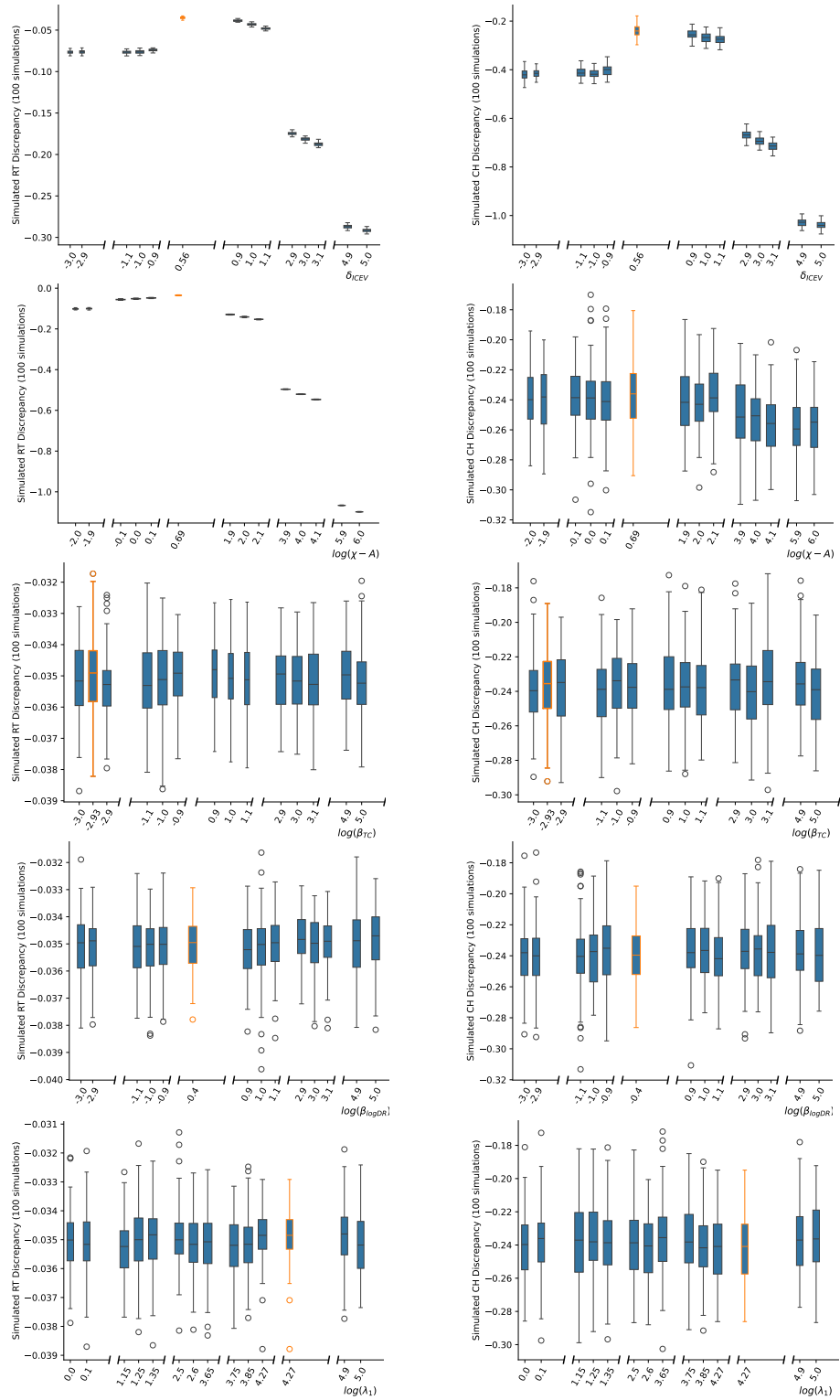


Figure 16: Boxplots for discrepancies over the domain of each parameter while others are fixed to MAP value. The boxplot with the orange line shows the discrepancies at MAP point.

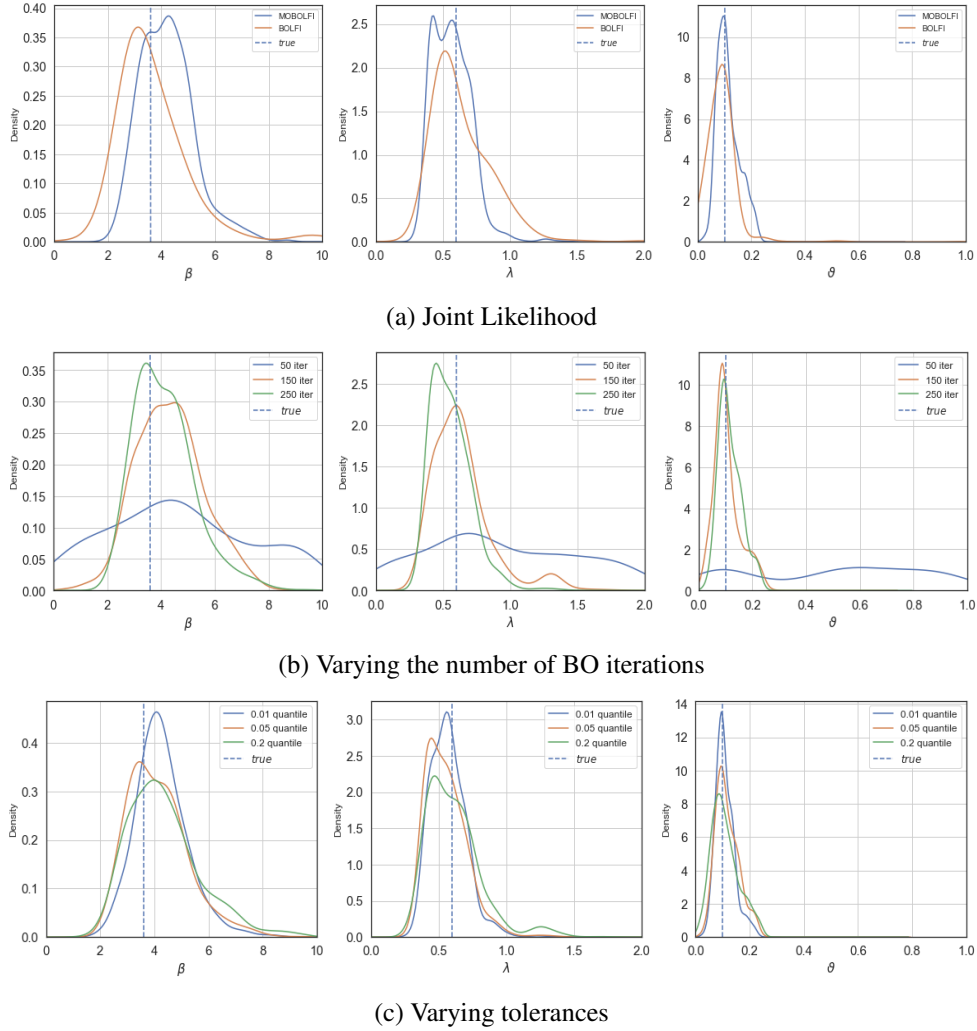


Figure 17: Approximate posteriors for the day care center example: (a) estimated posteriors using the joint likelihood, and the blue/orange curves show MOBOLFI/BOLFI approximate posterior; (b) estimated posteriors using varying number of BO iterations, and the blue/orange/green curves show MOBOLFI approximate posteriors with 250/150/50 BO iterations; (c) estimated posteriors for different tolerances and the blue/orange/green curves compare MOBOLFI approximate posteriors using 1%/5%/20% tolerance levels. The dashed blue lines show the location of the true parameter values. The approximate posteriors are kernel density estimates based on importance sampling.

D. Day care center example. Next we consider data from [Numminen et al. \(2013\)](#) measuring infections of bacteria strains over individuals in a number of day care centres. We refer the reader to [Numminen et al. \(2013\)](#) for a detailed description of the model. The data are indicators for whether individuals are infected with different strains at different times. We use the simplified model in Example 3, [Gutmann and Corander \(2016\)](#), and in their notation $R_s(t)$ is the rate of infection with strain s at time t . $R_s(t)$ is informed as a weighted sum of a probability for infection from within the day care centre (which may vary by strain and time) and a probability of infection from outside (which varies by strain). The weights in the weighted sum are unknown parameters, denoted β and Λ . There is a further unknown

parameter, which we denote by ϑ , which controls the relative rate of infection with strain s between situations when an individual is already infected with another strain, compared to when they are not. The set of all unknowns is $\theta = (\beta, \Lambda, \vartheta)$.

Following [Gutmann and Corander \(2016\)](#) we consider synthetic data where the the number of day care centres, the number of attendee individuals sampled in each day care center and the number of strains are set to 29, 36, 33 respectively. We generate the observed data from the model with $\theta^{\text{true}} = (3.6, 0.6, 0.1)$, and implement MOBOLFI with 50/150/250 BO iterations and tolerances set as 20%/5%/1% quantiles of the training data discrepancies. We consider the same four summary statistics $S = (S_1, S_2, S_3, S_4)^\top$ as [Numminen et al. \(2013\)](#), which can be computed for each daycare centre and averaged. The prior is the Uniform distribution illustrated in Example 8, [Gutmann and Corander \(2016\)](#). A discrepancy for BOLFI is then obtained by the Euclidean distance between simulated and observed summary statistics. For the MOBOLFI method, we consider two discrepancies: the first is the Euclidean distance between the first and fourth summary statistics for simulated and observed data, and the second is the Euclidean distance between the second and third summaries. The reason for this partitioning is that the first and fourth summaries represent diversity of prevalence of strains, and hence it could be beneficial to consider a discrepancy for these summaries separately. In this example, discrepancies are not scaled, yet a MAD scaling (see algorithm 1) is applied to the four data summaries in simulation. We consider approximate posterior densities obtained as kernel density estimates from an importance sampling with size 20000, and compare MOBOLFI approximate posterior densities with those obtained from BOLFI. The choice of auxiliary density for importance sampling has some flexibility, for results here we use a multivariate student-t distribution, with location middle points of the uniform prior and degree of freedom 3. No rejection criteria are used.

Figure 17 shows approximate BOLFI and MOBOLFI posteriors. In Figure 17a, the MOBOLFI approximate posterior exhibits similar variance compared to BOLFI. Figure 17b compares approximate posteriors trained with different numbers of BO iterations. With more training iterations, the approximate marginal posterior densities stabilize. Figure 17c shows approximate posteriors with different tolerance levels, using 250 BO iterations. Inference with a 1% quantile tolerance appears superior.